https://doi.org/10.5194/gmd-2020-148
Preprint. Discussion started: 17 July 2020

Geoscientific Model Development
Discussions
Open Access

Surface [Urban] Energy and Water Balance Scheme (v2020a) in non-urban areas: developments, parameters and performance

Hamidreza Omidvar[1,✉], Ting Sun[1], Sue Grimmond[1], Dave Bilesbach[2], Andrew Black[3], Jiquan Chen[4], Zexia Duan[5], Zhiqiu Gao[5,6], Hiroki Iwata [7], Joseph P. McFadden[8]

[1] Department of Meteorology, University of Reading, Reading, RG6 6BB, UK
[2] Biological Systems Engineering Department, University of Nebraska, Lincoln, NE, 68588, USA
[3] Faculty of Land and Food System, University of British Columbia, Vancouver, BC, V6T 1Z4, CA
[4] Center for Global Change and Earth Observation, Department of Geography, Michigan State University, East Lansing, MI, 48824, USA
[5] Collaborative Innovation Centre on Forecast and Evaluation of Meteorological Disasters, School of Atmospheric Physics, Nanjing University of Information Science and Technology, Nanjing, 210044, China
[6] State Key Laboratory of Atmospheric Boundary Layer Physics and Atmospheric Chemistry, Institute of Atmospheric Physics, Chinese Academy of Sciences, Beijing, 100029, China
[7] Department of Environmental Science, Faculty of Science, Shinshu University, Nagano 390-8621, Japan
[8] Department of Geography, University of California, Santa Barbara, CA, 93106 USA

✉ *Correspondence to*: *h.omidvar@reading.ac.uk; c.s.grimmond@reading.ac.uk*

ORCID IDs:

Hamidreza Omidvar: *https://orcid.org/0000-0001-8124-7264*
Ting Sun: *https://orcid.org/0000-0002-2486-6146*
Sue Grimmond: *https://orcid.org/0000-0002-3166-9415*
Dave Bilesbach: *https://orcid.org/0000-0001-8661-9178*
Andrew Black: *https://orcid.org/0000-0001-9292-1146*
Jiquan Chen: *https://orcid.org/0000-0003-0761-9458*
Zexia Duan: *https://orcid.org/0000-0003-2822-7066*
Zhiqiu Gao: *https://orcid.org/0000-0001-8256-005X*
Hiroki Iwata: *https://orcid.org/0000-0002-8962-8982*
Joseph P. McFadden: *https://orcid.org/0000-0002-5869-7774*

https://doi.org/10.5194/gmd-2020-148
Preprint. Discussion started: 17 July 2020

Geoscientific Model Development
Discussions

Abstract

This paper extends the applicability of the SUEWS (Surface [Urban] Energy and Water Balance Scheme) to extensive pervious areas (deciduous trees, evergreen trees, grass, croplands, soil and water) outside cities. It can be used either offline or online (i.e., coupled to weather/climate models). The required parameters to simulate the turbulent latent heat (or evaporative) flux are derived using observations. Both the parameters (leaf area index (LAI), albedo, roughness parameters and surface conductance) and the surface energy balance fluxes are evaluated at independent sites and/or different periods at the same site. Methods to obtain parameters and guidance to apply SUEWS are provided. Results demonstrate the impacts from differences in LAI dynamics and albedo for various types of vegetation. The relation between LAI and albedo is explored. Deciduous, evergreen, and grass land covers all have long periods of LAI maxima, but croplands normally have a short sharp peak due to harvesting. For most of the vegetation types studied the maximum albedo coincides with the maximum LAI period, but for some evergreen trees the maxima are associated with leaves changing colour (needles/leaves get darker as they age during autumn and winter). Ensuring these dynamics are captured is important for assessing urban-rural differences (e.g. canopy layer air temperature).

Keywords: SUEWS, pervious land cover, leaf area index, albedo, evaporation flux, roughness parameters

1 Introduction

Key to advancing our knowledge of planetary boundary layer behaviour is understanding surface-atmosphere interactions. Various land surface models (LSM) simulate these energy and water exchanges (Ek et al., 2003; Levis et al., 2004; Krinner et al., 2005; Kowalczyk et al., 2006). 'Urban' land use is amongst the most diverse (e.g. high-rise central business district to one-storey single family residential areas) with many land-cover types (e.g. paved roads, buildings, parks with trees and grass) influencing energy and water surface-atmosphere exchange through a wide range of complex biophysical processes. The complexity of urban systems have grown substantially with urbanization (United Nations 2018). A number of LSMs have been designed for urban areas (Grimmond et al., 2010), to capture processes such as heat and water released by anthropogenic activities (Grimmond et al., 1986; Grimmond, 1992; Masson, 2000; Kusaka et al., 2001; Martilli et al., 2002).

The Surface [Urban] Energy and Water Balance Scheme (SUEWS, Grimmond *et al.,* 1986, 1991, Grimmond & Oke 1991, Järvi *et al.,* 2011) characterises the heterogeneity of urban surfaces using seven land covers split between impervious (buildings, paved) and pervious

https://doi.org/10.5194/gmd-2020-148
Preprint. Discussion started: 17 July 2020

Geoscientific Model Development
Discussions

(evergreen trees/shrubs, deciduous trees/shrubs, grass, soil, water) types. SUEWS has been evaluated in multiple cities globally (e.g. Karsisto *et al.,* 2016, Ward *et al.,* 2016, Ao *et al.,* 2018, Kokkonen *et al.,* 2018, Harshan *et al.,* 2018) with varying mixes of integrated impervious-pervious land covers. However, when extensive areas of one type of pervious land cover (e.g. deciduous trees) occurs (e.g. in rural areas) some parameters are expected to differ from integrated-urban values (i.e. obtained for built-up areas). Most notably, there will be differences in parameters that are associated with the surface resistances for latent heat flux calculations because of differences in sub-grid-scale advection processes (Spronken-Smith et al., 2000). Thus, new parameters need to be determined from observations.

Our objective is to bridge this gap by deriving values for several latent heat flux related parameters (*viz*, leaf area index (LAI), albedo, roughness parameters and surface resistance) for extensive non-urban pervious areas and assess their seasonal variability. This improves SUEWS regional applicability with rural areas with forests, farms, and grasslands (*etc.*). For reproducibility and applicability to other data sets parameter derivation is implemented in Python Jupyter notebooks (Omidvar et al., 2020). The SUEWS model (Sect. 2.1, Appendix A) is used with observations (Sect. 2.2) from numerous sites. Methods address both obtaining the parameters and their evaluation (Sect. 2.3). The derived parameters (Sect. 3) are evaluated (Sect. 4), allowing conclusions to be drawn (Sect. 5).

2 Methods

2.1 SUEWS and its vegetation-related sub-models

The details of how SUEWS computes the surface energy, water and carbon fluxes are given in Järvi *et al.* (2011), Ward *et al.* (2016), and Järvi *et al.* (2019). The surface energy and water balances are directly linked by the turbulent latent heat flux (Q_E) or its mass equivalent evaporation (*E*):

$$Q^* + Q_F = Q_H + Q_E + \Delta Q_S \quad (1)$$

$$P + I_e = E + R + \Delta S \quad (2)$$

where Q^* is the net all-wave radiation flux, Q_F is the anthropogenic heat flux, Q_H is the turbulent sensible heat flux, ΔQ_S the net storage heat flux, and P, I_e, ΔS and R are precipitation, external water use, net change in the canopy water storage and runoff, respectively. As we focus on extensive (non-urban) pervious areas the anthropogenic heat flux (Q_F) is assumed to be 0 W m^{-2}.

https://doi.org/10.5194/gmd-2020-148
Preprint. Discussion started: 17 July 2020

Geoscientific Model Development
Discussions

Vegetation phenology changes key model parameters, most notably, leaf area index (*LAI*). Leaf-out and senescence impact the albedo (α) and therefore surface radiative exchanges. LAI changes also modify both aerodynamic roughness parameters (roughness length (z_0), zero plane displacement height (z_d)) (e.g. Kent *et al.,* 2017) and surface resistance (r_s) . The former impacts aerodynamic resistance (r_a) while r_s directly moderates Q_E (Sect. 2.1.4).

Model parameters need to be internally consistent for land cover type *i.* This allows different types of vegetation (e.g. a crop) to be simulated. All the parameters needed for a vegetated surface and those addressed in this paper are given in Table 1. SUEWS allows parameters to vary between individual grids (Järvi *et al.,* 2019, Sun *et al.,* 2020) and thus can represent a high degree of spatial heterogeneity (e.g. different heights of trees).

Table 1: Parameters that SUEWS uses (and can be set) for pervious surface types by first associated process (i.e. most impact multiple variables). Those determined (D) in this study (*) and the values used (given in Table: T#, Sect.: S#) in individual equations (E).

Category	Symbol	Definition	Value	E	D
Radiation	$\alpha_{LAI_{\min}}$	Albedo at LAI_{min}	T4	6	*
	$\alpha_{LAI_{\max}}$	Albedo at LAI_{max}	T4	6	*
	ε_0	Emissivity	T2		
Leaf Area Index (LAI)	LAI_{min}	LAI Minimum	T4	4,5	*
	LAI_{max}	LAI Maximum	T4	4.5	*
	$T_{BaseSDD}$	Base temperature senescence degree days (*SDD*)	T4	4	*
	$T_{BaseGDD}$	Base temperature for growing degree days	T4	4	*
	GDD_v	GDD from the start of the crop vegetative phase	T4	5	*
	$GDD_{LAI_{max}}$	Growing degree days until LAI_{max}	T4	5	*
Roughness	H_v	Vegetation height	T3		
	z_{0m}	Roughness length for momentum	S2.1.4	9	*
	z_d	Zero plane displacement	S2.1.4	9	*
Surface resistance	*G2-G6*	Coefficients	T5	12	*
	G_{max}	Coefficients	T5	12	*
	T_H, T_L	Temperature limits for switching off evaporation	S2.1.4	15	
	s_1	Coefficient related to wilting point	S2.1.4	16	
	$K_{\downarrow,\max}$	Maximum observed incoming shortwave	S2.1.4	13	
Storage heat flux	a_1-a_3	Coefficient for storage heat flux	T2	7	*
Water storage	S_i	Canopy water storage capacity	T2	19	

2.1.1 Leaf Area Index (*LAI*)

In SUEWS, LAI for the current day (d) is calculated using cumulative growing degree days (GDD) and senescence degree days (SDD) of the previous day ($d-1$) for vegetation type *i.* For forests and grass we use (Järvi *et al.,* 2011):

https://doi.org/10.5194/gmd-2020-148
Preprint. Discussion started: 17 July 2020

$$LAI_{d,i} = \begin{cases} \min\left(LAI_{\max,i}, LAI^{\omega_1}_{d-1,i} GDD\ \omega_2 + LAI_{d-1,i}\right), & T_{BaseSDD} < T_d < T_{BaseGDD} \\ \max\left(LAI_{\min,i}, LAI^{\omega_1}_{d-1,i} SDD\ \omega_2 + LAI_{d-1,i}\right), & T_{BaseGDD} < T_d < T_{BaseSDD} \end{cases} \quad (3)$$

with $\omega_1 = 30 \times 10^{-3}$ and $\omega_2 = 0.5 \times 10^{-3}$. The base temperatures associated with the initiation of leaf-on ($T_{BaseGDD}$) and leaf-off ($T_{BaseSDD}$, units °C) periods are used relative to a mean air temperature T_d derived from the daily maximum ($T_a^{\max}$) and minimum ($T_a^{\min}$) for the current day:

$$T_d = \frac{T_a^{\max} + T_a^{\min}}{2} \quad (4)$$

The model requires the maximum and minimum *LAI* values ($LAI_{max,i}$, $LAI_{min,i}$) for each vegetation type. Eq. 3 has fewer calibration parameters than Eq. A1 of Järvi *et al.* (2014) as $T_{BaseGDD}$ and $T_{BaseSDD}$ are determined for each site (Sect. 2.3). If $T_{BaseGDD}$ and $T_{BaseSDD}$ are available for a site, one should account for day-length and photoperiod for more northerly sites (Bauerle et al., 2012; Gill et al., 2015).

For crops (e.g. rice, wheat) *LAI* also depends on the planting date. However, as crops are grown to be harvested, the period of LAI_{max} is short (cf. e.g. forests as parametrised in Eq. 3). We propose:

$$LAI_{d,crop} = \begin{cases} \min\left(LAI_{\max}, \dfrac{LAI_{max} - LAI_{min}}{GDD_{LAI_{max}} - GDD_v}\left(GDD_p - GDD_v\right) + LAI_{\min}\right) & GDD_p \leq GDD_{LAI_{max}} \\ \max\left(LAI_{\min}, -\dfrac{LAI_{max} - LAI_{min}}{GDD_{LAI_{max}} - GDD_v}\left(GDD_p - GDD_v\right) + 2LAI_{max} - LAI_{\min}\right) & GDD_p > GDD_{LAI_{max}} \end{cases} \quad (5)$$

where GDD_p is the *GDD* accumulated from the day of planting; $GDD_{LAI_{max}}$ is associated with LAI_{max} and GDD_v is the start of crop vegetative phase. Note that GDD, SDD, and GDD_p (in Eq. 4 and 5) change with time from their base temperatures ($T_{BaseGDD}$ for GDD, $T_{BaseSDD}$ for SDD, 0 °C for GDD_d). Using a different base temperature (than 0 °C) to calculate GDD_d, GDD_v, and $GDD_{LAI_{max}}$ in Eq. 5 leads to same $LAI_{d,crop}$ results as only the difference values $GDD_{LAI_{max}} - GDD_v$ and $GDD_p - GDD_v$ are important. Here, these crop specific coefficients are obtained for rice and winter wheat (Sect. 2.3).

2.1.2 Albedo (α)

In SUEWS, the albedo varies with daily LAI between the minimum ($\alpha_{LAI_{\min}}$) and maximum ($\alpha_{LAI_{\max}}$) by vegetation type:

$$\alpha_{d,i} = \alpha_{d-1,i} + \left(\alpha_{LAI_{\max},i} - \alpha_{LAI_{\min},i}\right)\frac{LAI_{d,i} - LAI_{d-1,i}}{LAI_{\max,i} - LAI_{\min,i}} \quad (6)$$

https://doi.org/10.5194/gmd-2020-148
Preprint. Discussion started: 17 July 2020

Geoscientific Model Development Discussions

The maximum albedo does not necessarily occur with the maximum LAI because of change in leaf/needle colour (Sect. 3.1). Here we focus on snow-free conditions, albeit a snow module is available in SUEWS (Järvi *et al.,* 2014). Bare soil and water albedo are assumed to be constant in a model run (Sect. 3.2).

The observed (30 min) incoming and outgoing shortwave radiation are used to calculate each albedo from 10:00 to 14:00 (local standard time). From this, one mean albedo for each day is calculated. The two model parameters (Eq. 6, Table 1) are selected from those that minimize the mean absolute error (MAE, Sect. 2.4) of the albedo prediction at a calibration site.

Within SUEWS the albedo is used with the observed incoming shortwave radiation to obtain Q^*. In the current analyses, the observed incoming longwave ($L_\downarrow$) and modelled outgoing longwave radiation ($L_\uparrow = (1-\varepsilon_0)L_\downarrow + \varepsilon_0\sigma T_s^4$ where ε_0 is the surface emissivity, σ is the Stefan Boltzmann constant ($\mathrm{W\,m^{-2}\,K^{-4}}$), and T_s is the surface temperature (K), Appendix A.1) are used. Table 2 gives the emissivity values used.

To determine $\alpha_{LAI_{\min}}$ and $\alpha_{LAI_{\max}}$ for each individual vegetated site (excluding snow) we analyse observational data for snow free periods. Although SUEWS has a snow option, this option is disabled in all runs to verify "no snow" scenarios. We assume precipitation is snow if $T_a < 0$ °C (Järvi *et al.,* 2014), and that snow remains until the 5-day moving average of air temperature is above 5 °C. Although this method will not flag all the snow-covered days (e.g. duration of snow cover also depends on snow depth), it provides a rough estimate of when the albedo is affected by snow.

Table 2: Pervious surface OHM storage heat flux (a_1, a_2, a_3) coefficients are derived (this study O20, methods: Sect. 2.1.3), except for tree and grass areas which are derived from literature sources (D85= Doll *et al.* (1985), M85= McCaughey (1985)*) by Grimmond et al. (1991) and Grimmond and Oke (1999)); canopy water storage (S_i, Eq. 19) from B03= Breuer et al. (2003), and emissivity from sources in W16 - Ward et al. (2016).*

Vegetation Type	a_1	a_2	a_3	Source	S_i *(mm)*	Source	Emissivity	Sources in
Deciduous trees/shrubs	0.215	0.325	-19.9	M85	1.3	B03	0.98	W16
Evergreen trees/shrubs	0.215	0.325	-19.9	M85	0.8	B03	0.98	W16
Grass	0.215	0.325	-19.9	D85	1.9	B03	0.93	W16
Rice	0.185	0.615	-18.0	O20	1.9	B03	0.95	Water
Wheat	0.283	0.784	-18.0	O20	1.9	B03	0.93	Grass
Soil	0.210	0.902	-20.4	O20	1.9	B03	0.93	W16
Water	0.880	0.370	-85.4	O20	-	-	0.95	W16

https://doi.org/10.5194/gmd-2020-148
Preprint. Discussion started: 17 July 2020

Geoscientific Model Development
Open Access
Discussions

2.1.3 Storage heat flux (ΔQ_S)

Storage heat flux is simulated with the objective hysteresis model (OHM, Grimmond *et al.,* 1991):

$$\Delta Q_S = \sum_i f_i \left[a_{1,i} Q^* + a_{2,i} \frac{\partial Q^*}{\partial t} + a_{3,i}\right] \tag{7}$$

where f_i is the plan area (or 3d, Grimmond et al. 1991, Grimmond and Oke 1999) fraction of surface i and $a_{1\text{-}3}$ are the OHM coefficients (Table 2). To obtain $a_{1\text{-}3}$ from observations of Q^* and ΔQ_S (as the residual of Eq. 1, in extensive pervious sites Q_F = 0 W m^{-2}) regression is used. As the sites are assumed to be extensively the same pervious land cover type f_i = 1 in each case. We determine one set of OHM coefficients per site, hence assuming they are constant and ignoring soil wetness effects and other variations.

2.1.4 Latent heat flux (Q_E)

In SUEWS, a modified Penman-Monteith equation (Penman, 1948; Monteith, 1965) is used to compute Q_E with Q_F = 0 W m^{-2} in non-urban areas (e.g. this paper) and greater than zero for cities (Grimmond & Oke 1991):

$$Q_E = \frac{s(Q^* + Q_F - \Delta Q_S) + \frac{\rho c_p V}{r_a}}{s + \gamma\left(1 + \frac{r_s}{r_a}\right)} \tag{8}$$

The atmospheric state is obtained from the slope of saturation vapour pressure curve with respect to temperature (s, units: Pa K^{-1}), density of air (ρ, kg m^{-3}), specific heat of air at constant pressure (c_p, J K^{-1} kg^{-1}), vapour pressure deficit (V, Pa), psychrometric 'constant' (γ,: Pa K^{-1}), and the aerodynamic resistance for water vapour (r_a, units: s m^{-1}). The latter is obtained from Ulden & Holtslag (1985) and Järvi *et al.* (2011):

$$r_a = \frac{\left[\ln\left(\frac{z_m - z_d}{z_{0m}} - \psi_m(\zeta)\right)\right]\left[\ln\left(\frac{z_m - z_d}{z_{0v}} - \psi_v(\zeta)\right)\right]}{\kappa^2 u}, \tag{9}$$

where z_m is the measurement height for mean wind speed (u) and κ the von Kármán constant (0.4 assumed); the aerodynamic parameters z_d (zero plane displacement height) and z_{0m} (roughness length for the momentum) are estimated as a function of canopy height which varies for different *LAI* states of each surface, as discussed in Appendix B (Garratt, 1994; Grimmond and Oke, 1999). For water and soil surfaces they are estimated to be z_{0m} = 0.0005 m and 0.002 m respectively with z_d = 0 m (Moene and van Dam, 2013). Canopy height for the different surface types is given in Table 3. The stability scale ζ ($= (z_m - z_d)/L$) depends on L the Obukhov length. SUEWS is modified (Appendix A) so that for completely pervious surfaces the

https://doi.org/10.5194/gmd-2020-148
Preprint. Discussion started: 17 July 2020

roughness length for vapour (z_{0v}) is calculated as $z_{0v} = 0.1z_{0m}$ (Brutsaert, 1982) and assumed to be the same as for sensible heat. The atmospheric stability functions of momentum (ψ_m) and water vapour (ψ_v) for unstable condition are (Campbell and Norman, 1998):

$$\psi_v = 2\ln\left[\frac{1+(1-16\zeta)^{1/2}}{2}\right], \quad \psi_m = 0.6\psi_v \tag{10}$$

and for stable condition (Campbell and Norman, 1998; Högström, 1988):

$$\psi_v = -4.5\ln(1+\zeta), \quad \psi_m = -6\ln(1+\zeta) \tag{11}$$

For completely wet surfaces, the surface resistance (r_s) is assumed to be 0 s m^{-1} (i.e. potential evaporation is calculated from Eq. 8). Otherwise r_s, or its inverse surface conductance (g_s), is modelled (Ward *et al.,* 2016):

$$r_s^{-1} = g_s = \sum_i (g_{\max,i} f_i) g(LAI_i) g(K_\downarrow) g(\Delta q) g(T_a) g(\Delta\theta_{soil}) \,. \tag{12}$$

To reduce the number of coefficients in Ward *et al.*'s (2016), G_1 (their Eq. 9) is removed from the first term (of Eq. 12) leaving $g_{\max,i}$ (maximum surface conductance, units: m s^{-1}) and f_i. For 'homogeneous' sites (Sect. 2.2) f_i =1. Phenological state is critical: $g(LAI_i) = \frac{LAI_i}{LAI_{\max,i}}$. For bare soil surfaces (i.e. no vegetation), when *LAI* is irrelevant $g(LAI_i) = 1$. The remaining terms are related to meteorology (incoming shortwave radiation $K_\downarrow$, specific humidity deficit Δq, air temperature T_a), and soil moisture deficit ($\Delta\theta_{soil}$, difference between soil moisture and soil water capacity); using Grimmond & Oke (1991), Järvi *et al.* (2011), and Ward *et al.* (2016):

$$g(K_\downarrow) = \frac{\dfrac{K_\downarrow}{G_2 + K_\downarrow}}{\dfrac{K_{\downarrow,\max}}{G2 + K_{\downarrow,\max}}} \tag{13}$$

where $K_{\downarrow,\max}$ is the maximum observed incoming shortwave radiation (= 1200 W m^{-2});

$$g(\Delta q) = G_3 + (1 - G_3)G_4^{\Delta q} \tag{14}$$

$$g(T_{air}) = \frac{(T_{air} - T_L)(T_H - T_a)^{T_c}}{(G_5 - T_L)(T_H - G_5)^{T_c}} \tag{15}$$

where $T_c = \frac{T_H - G_5}{G_5 - T_L}$ is a function of the lower ($T_L = -20$ °C) and upper (T_H= 55 °C) limits that determine when the evaporation switches off in SUEWS. Here we extended T_L from -10 °C (from Ward *et al.,* 2016) to -20 °C to ensure that the temperature limit covers all climates (Table 3) studied here. Note Q_E is negligible (Appendix C) when $T_a < -20$ °C.

https://doi.org/10.5194/gmd-2020-148
Preprint. Discussion started: 17 July 2020

The soil moisture control considers the wilting point ($\Delta\theta_{WP} = \frac{s_1}{G_6}$, with $s_1 = 5.56$, see Järvi *et al.* 2011) using G_6 to vary with soil and plant type:

$$g(\Delta\theta_{soil}) = \frac{1-\exp(G_6(\Delta\theta_{soil}-\Delta\theta_{WP}))}{1-\exp(-G_6\Delta\theta_{WP})} \tag{16}$$

To obtain the G_2 *to* G_6 and $g_{\max}$, a so-called 'observed' g_s is obtained by rearranging Eq. 8, when the surface is dry (and both Q_H and Q_E are > 0 W m^{-2}):

$$\frac{1}{g_s} = r_s = \left[\frac{s}{\gamma}\frac{Q_H}{Q_E} - 1\right] r_a + \frac{\rho c_p V}{\gamma Q_E}. \tag{17}$$

The g_s related parameters (Eq. 12) are obtained using non-linear regression with the observed values (Eq. 17). We use a Python package Platypus (Hadka, 2015) with a multi-objective evolutionary algorithm (Zhou et al., 2011) so that we capture: (1) *variations of* g_s: difference between standard deviation of g_s from model and observations (normalized by standard deviation of observations); and (2) *magnitude of* g_s: mean absolute difference between g_s from model and observations.

SUEWS has a running water balance that accounts for the multiple surface types. The amount of water on the canopy of each surface (C_i) (Grimmond & Oke 1991) is used to vary the surface resistance between dry and wet ($r_s = 0$ s m^{-1}) by replacing r_s with r_{ss} (Shuttleworth 1978):

$$r_{\mathrm{ss}} = \left[\frac{W}{r_b(s/\gamma+1)} + \frac{(1-W)}{r_s + r_b(s/\gamma+1)}\right]^{-1} - r_b(s/\gamma+1), \tag{18}$$

where W is a function of the relative amount of water present on each surface to its water storage capacity (S_i, Table 2):

$$W = \begin{cases} W = 1 & C_i \geq S_i \\ \dfrac{K-1}{K - S_i/C_i} & C_i < S_i \end{cases}. \tag{19}$$

K depends on the aerodynamic and surface resistances:

$$K = \frac{(r_s/r_a)/(r_a - r_b)}{r_s + r_b(s/\gamma+1)}, \tag{20}$$

where r_b, the boundary layer resistance, is a function of friction velocity u_* (Shuttleworth 1983):

$$r_b = 1.1u_*^{-1} + 5.6u_*^{\frac{1}{3}}. \tag{21}$$

Equations 18-21 ensure that the surface resistance r_{ss} has a smooth transition from 0 (a completely wet surface) to r_s (a dry surface).

https://doi.org/10.5194/gmd-2020-148
Preprint. Discussion started: 17 July 2020

2.2 Observations and sites

To determine parameters for non-urban surfaces (Table 1), and to evaluate their performance, observations from "homogeneous" sites with long term radiation fluxes and eddy covariance measurements are required (Table 3). The 30 min meteorological observations used are air temperature, incoming shortwave radiation, upwelling shortwave radiation, station pressure, relative humidity, wind speed, precipitation, net all-wave radiation, sensible heat flux and evaporation flux. The precipitation data are used to select dry periods and are required by SUEWS to calculate $\Delta\theta_{soil}$ and the surface state (C_i).

The site land cover characteristics are provided by their key references (Table 3). The observed LAI data are from the NASA Moderate Resolution Imaging Spectroradiometer (MODIS, Nishihama *et al.,* 1997) four-day composite product MCD15A3H (Myneni *et al.,* 2015) with 500 m resolution.

The sites (Fig. 1) in North America are part of the AmeriFlux network (Baldocchi *et al.,* 2001) and two of the Asian sites are part of AsiaFlux (AsiaFlux, data access: 2020-01-22). Seven land cover types are analysed (Table 3) using one to three sites:

(1) Deciduous trees (DBF): three sites
(2) Evergreen trees (ENF): three sites
(3) Grass (GRA): two sites
(4) Rice (RIC): two sites
(5) Winter wheat (WHT): one site
(6) Water (WAT): one continuous and two intermittent flood irrigated rice sites (Table 3)
(7) Bare soil (BSV): two sites (up to four weeks after rice planting).

Irrigation (I_e, Eq. 2) modifies both the soil moisture deficit and surface state and is critical for the growth of many plants. Notably rice has flood irrigation for a period when a site-specific depth (Table 3) is maintained. At CN-DNT (Table 3) this occurs until 5 weeks before harvest, whereas at PH-IRI there are only 2 weeks without irrigation. The CN-DNT wheat field is kept saturated but not flooded for the entire time (Duan *et al*., 2020). To account for this, sufficient water is added by SUEWS to satisfy these conditions (Appendix A.2 gives details).

Table 3: Analysed pervious land cover types (DBF: Deciduous Broadleaf Forests, ENF: Evergreen Needleleaf Forests, GRA: Grasslands, CRP: crops, BSV: bare soil, WAT: Water) at different sites and periods. Key references and DOI provide the details of the observations and each site. The sites elevation (elev) above sea level (asl), vegetation height (H_v) above ground level (agl) and height of

https://doi.org/10.5194/gmd-2020-148
Preprint. Discussion started: 17 July 2020

Geoscientific Model Development
Discussions
Open Access
EGU

wind speed measurement (H_U). Sites are in Canada (CA), China (CN), Japan (JP), Philippines (PH) and USA (US). At CN-DNT both rice (RIC) and wheat (WHT) are grown.

Site	Name	Type	Mean Temp. (°C)[1]	Elev. (m asl)	H_v (m agl)	H_U (m agl)	Lat. (°N)	Lon. (°)	Calibration year	Test years	DOI	Key Reference
US-MMS	Morgan Monroe State Forest	DBF	13.2	275.0	25.0	46.0	39.32	−86.41	2017	2010,2012, 2016	10.17190/AMF/1246080	Schmid *et al.* (2000)
US-UMB	Univ. Michigan Biological Station	DBF	7.1	234.0	20.0	46.0	45.56	−84.71	2008	2010,2014, 2016	10.17190/AMF/1246107	Curtis *et al.* (2002)
US-Oho	Oak Openings	DBF	11.0	230.0	24.0	34.0	41.55	−83.84	2010	2011,2012, 2013	10.17190/AMF/1246089	Noormets *et al.* (2008)
CA-Obs	Saskatchewan - Western Boreal, Mature Black Spruce	ENF	1.3	628.9	7.2	26.0	53.99	−105.12	2008	2003,2005, 2006	10.17190/AMF/1375198	Bergeron *et al.* (2007)
CA-Qcu	Quebec - Eastern Boreal, Black Spruce /Jack Pine Cutover	ENF	1.6	392.3	13.8	24.0	49.27	−74.04	2010	2005,2008, 2009	10.17190/AMF/1246828	Bergeron *et al.* (2007)
US-Blk	Black Hills	ENF	6.6	1718.0	13.0[2]	24.0	44.16	−103.65	2005	2004,2006, 2008	10.17190/AMF/1246031	-
US-KUT	KUOM Turfgrass Field	GRA	8.0	301.0	0.07	1.35	44.99	−93.19	2008	2006,2007	10.17190/AMF/1246145	Peters et al. (2011)
US-AR1	ARM USDA UNL OSU Woodward Switchgrass 1	GRA	15.6	611.0	1.0[3]	2.84	36.43	−99.42	2012	2010,2011	10.17190/AMF/1246137	-
CN-DNT	Rice-wheat rotation cropland Dongtai country, Jiangsu	CRP, BSV[4]	15.1	4.0	0.6 (R) 0.5 (W)	10.0	32.76	120.47	2015 (R)[5] 2015-16 (W)[6]	2016 (R) 2014-15 (W)	-	Duan *et al.* (2020)
JP-SWL	Suwa Lake site Suwa city, Nagano	WAT	14.6	759.0	-	3.0	36.04	138.10	April 2015	May-Dec 2015	www.asiaflux.net	Iwata *et al.* (2018)
PH-IRI	Los Banos, Laguna	CRP, BSV[4]	27.5	21.0	1.0	2.25	14.2	121.3	2014[7]	2013	www.asiaflux.net	Alberto *et al.* (2009)

1 For years used in this study
2 Source: Keyser *et al.* (2008)
3 Estimated from Porter (1966)
4 First 4 weeks after planting rice - considered as soil surface.
5 Rice planted and harvested: Jun 20-Nov 7 in 2015 and Jun 16-Nov 5 in 2016. Field flooded (0.15 m) until 5 weeks prior to harvest.
6 Wheat planted and harvested: Dec 15-May 31 in 2014-15 and Dec 10-May 25 in 2015-16. Field kept saturated the entire period.
7 Rice planted and harvested: Jun 27-October 22 in 2013 and Jun 17-Oct 1 in 2014. Field flooded (0.3 m) until 2 weeks prior to harvest.

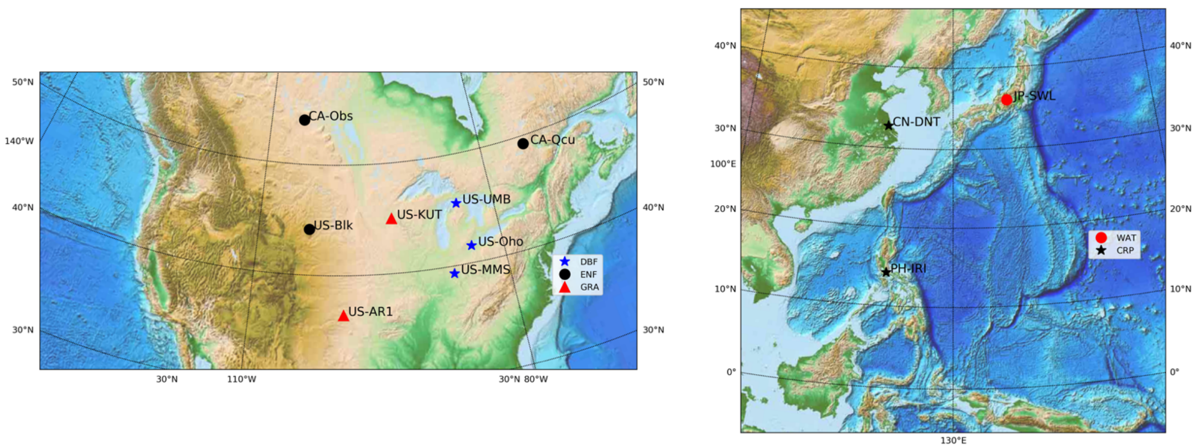

Figure 1: Location of sites (Table 3) analysed by vegetation type deciduous trees (DBF), evergreen trees (ENF), grass (GRA), water (WAT) and crops (CRP). Source of base maps: Basemap (2012)

https://doi.org/10.5194/gmd-2020-148
Preprint. Discussion started: 17 July 2020

2.3 Determination of SUEWS parameters for pervious surfaces

The processes and parameters of interest (Sect. 2.1, Table 1) are not completely independent for vegetated surfaces as both LAI and albedo influence surface conductance, hence Q_E. As LAI varies with vegetation type, season and climate (e.g. latitude, local site characteristics), this should be determined prior to albedo, surface conductance and Q_E; whereas neither bare soil nor water surfaces require *LAI* (Fig. 2). At each site, the LAI and albedo model parameters are derived with one year of data ('calibration') and evaluated with other years ('test') (Table 3, Fig. 3). Given limited data for the water site (JP-SWL, Table 3) the albedo is determined for April 2015 and evaluated for the remaining months (Fig. 3). Calibration data are used to derive z_0 and z_d (Eq. 9) using the methods in Appendix B. These values are used in the Q_E evaluation.

To assess the generality of the derived parameters (chosen based on minimized MAE) for a surface type, most are evaluated against both (Fig. 3): (a) another year at the same site, and (b) two independent sites using one year of data. However, lack of data prevents this for bare soil, crop, and water sites.

The Python package SuPy v2020.3.18 (Sun & Grimmond 2019) with the calculation kernel SUEWS v2020a (Sun et al., 2020 ,Appendix A) is used for all simulations. The 5-min simulations are averaged to 30-min for consistency with the eddy covariance observations (Table 3). The complete Python source code (with comments) are provided at Omidvar et al. (2020).

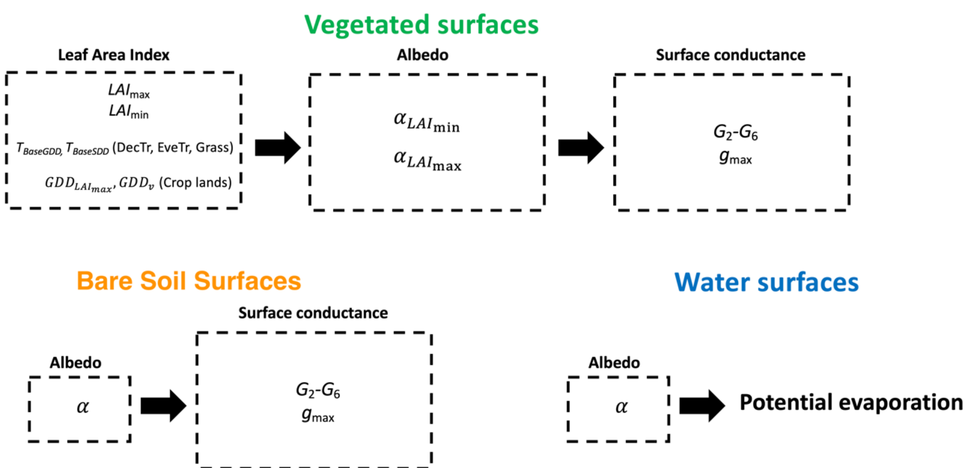

Figure 2: To obtain SUEWS parameters for LAI, albedo and surface conductance, the order indicated is required to be used. For notation see Table 1

https://doi.org/10.5194/gmd-2020-148
Preprint. Discussion started: 17 July 2020

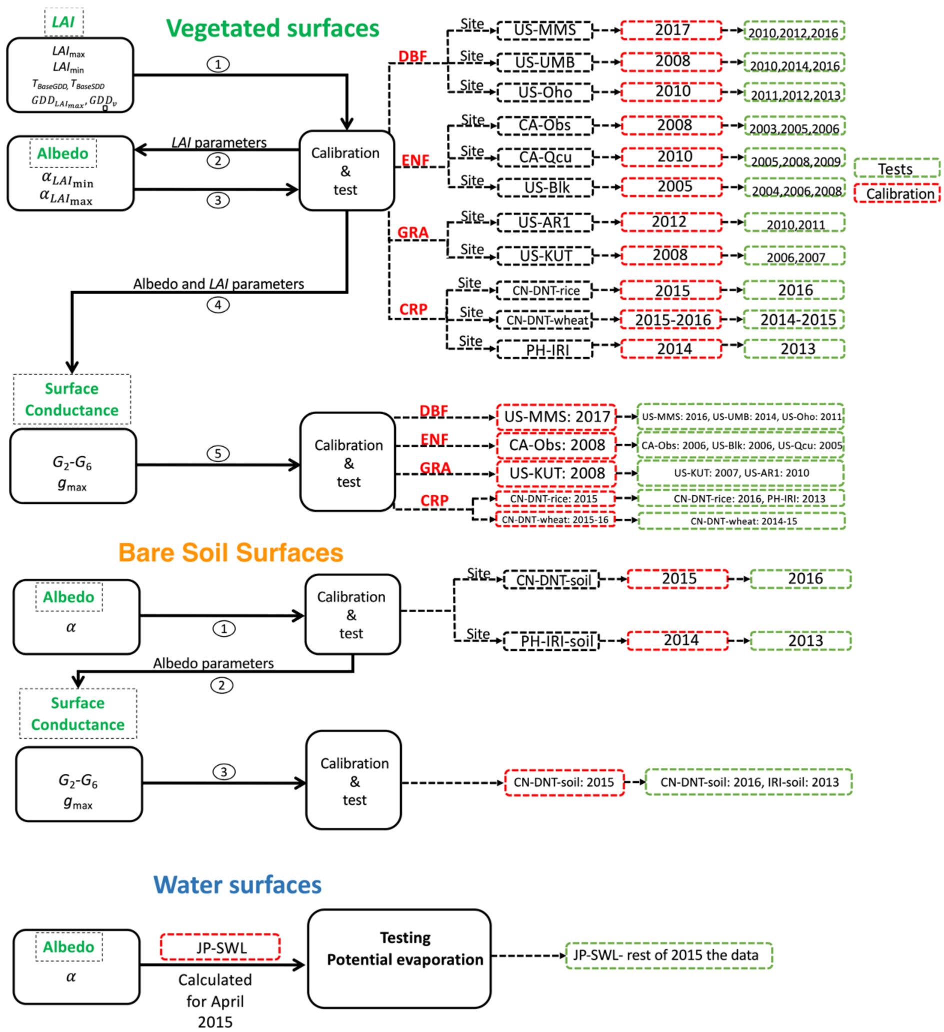

Figure 3: Sites and periods (Table 3) used to derive (calibrate) and evaluate (test) the parameters related to LAI, albedo and surface conductance for non-urban land types. Numbers in circles indicate order of calculation. Notation defined in Table 1.

2.4 Evaluation metrics

To evaluate the model output (Y_{mod}) with observations (Y_{obs}) for a number (N) of data points the following metrics are used:

1) mean absolute error (MAE):

$$\mathrm{MAE} = \frac{\sum_{i=1}^{n} |Y_{mod} - Y_{obs}|}{N} \tag{22}$$

https://doi.org/10.5194/gmd-2020-148
Preprint. Discussion started: 17 July 2020

2) mean bias error (MBE):

$$\text{MBE} = \frac{\sum_{i=1}^{n}(Y_{mod} - Y_{obs})}{N} \tag{23}$$

Both the MAE and MBE are ideally 0 (with units of parameter/variable assessed).

3) normalised MAE (nMAE):

$$\text{nMAE} = \frac{\text{MAE}}{\text{MAE}_{calib}} \tag{24}$$

This is used to assess the model performance relative to data used to derive the parameters (calib). If nMAE > 1 the performance is poorer with the test data set than the calibration set (and vice versa).

To evaluate the evaporation, data are stratified by *LAI* phenology: (1) leaf off/leaf on/transition for DBF, ENF and GRA sites (Sect. 3.1, 3.3) and (2) vegetative/reproductive/ripening for crops. Crop dates are available for CN-DNT (Table 3) but not for PH-IRI-rice. As different states are not available for the PH-IRI-rice, BSV and WAT sites Q_E evaluation uses the entire period.

3 Results and Discussion

3.1 *LAI* parameters

Fig. 4 shows how different parameters control the *LAI* dynamics (Eq. 3) at the deciduous forest site US-MMS (Table 3, Fig. 1) in 2017. At this site, *LAI* begins to increase from its minimum (0.5 m^2 m^{-2}) as the daily mean air temperature (T_d) increases. As T_d increases above $T_{BaseGDD}$ *LAI* increases to its maximum (i.e. 5). *LAI* remains constant until T_d goes below $T_{BaseSDD}$ when *LAI* starts decreasing until it reaches the minimum (i.e. 0.5). Whereas for rice (Fig. 5, CN-DNT site) the *LAI* evolution from planting has a short peak period with almost symmetric ascending and descending parts. Given this different behaviour in *LAI* evolution between crops and other vegetation types, two different forms (Eq. 3 and 5) are used.

Across all sites and years, the calculated *LAI* (Eq. 3, Table 4 parameters) have good agreement with the MODIS *LAI* product (Sect. 2.1.1) (Fig. 6, 7). Based on entire years, all MAE are less than 0.67 m^2 m^{-2} and the MBE are between −0.36 and 0.16 m^2 m^{-2} (Table D1). The largest deviation from the MODIS *LAI* occurs at a grassland site (US-AR1) in 2011. A possible explanation for this may be a lack of rain, as in 2011, US-AR1 received half the rainfall of the other years, leading to larger soil moisture deficits (cf. 2010, 2012 (calibration)) (Fig. 8). This

https://doi.org/10.5194/gmd-2020-148
Preprint. Discussion started: 17 July 2020

important role of rainfall and soil moisture in moderating *LAI* dynamics with shallow vegetation roots is also found by Bobée *et al.* (2012).

As expected, deciduous tree (DBF) sites have the largest variation in *LAI* among the vegetated areas whereas grass has the smallest (Fig. 6, Table 4). However, the *LAI* variation at the evergreen sites (ENF) indicates that assuming a constant *LAI* would result in poor predictions of albedo and consequently turbulent heat fluxes. Consistent with Liu *et al.* (2013) and Alemu & Henebry (2016), for each vegetation type $T_{BaseGDD}$ and $T_{BaseSDD}$ generally decrease with increase in latitude (Table 3, 4). However, CA-Obs has slightly larger values than CA-Qcu despite its higher latitude.

For both rice and wheat Eq. 5 performs well (Fig. 9, Table D1). The sharp decrease of *LAI* after its peak in both rice and wheat is captured (Fig. 9a-c). For these crops, the MAE is < 0.53 m^2 m^{-2} and MBE is between -0.31 and 0.19 m^2 m^{-2}.

Generally, both Eq. 3 and 5 perform similarly when derived and evaluated (Fig. 7c, 9d). This suggests the *LAI* calibration parameters from other years can be used. Recommended values are given in Sect. 4. Although Eq. 3 performance varies between calibration and test sites with phenology, no general trend is found (Fig. 7c).

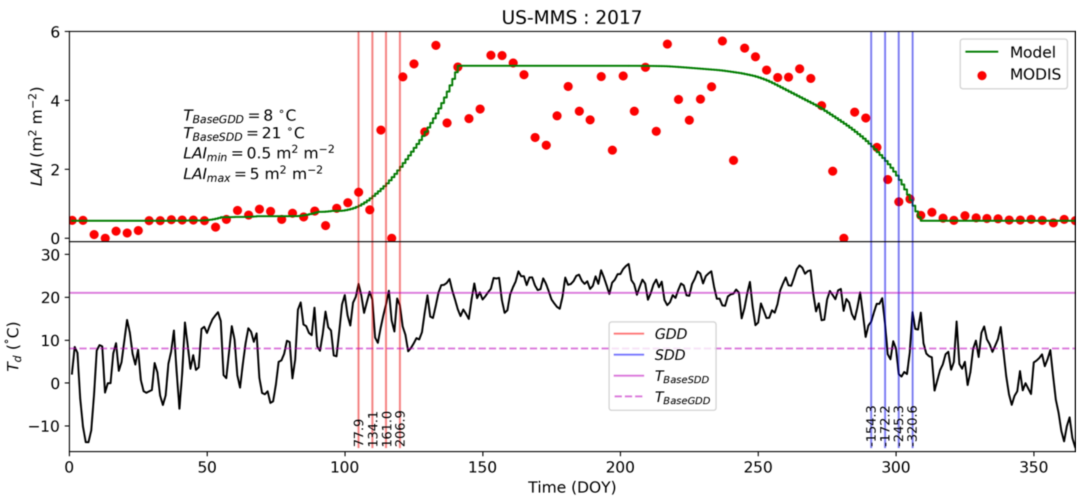

Figure 4: Deciduous forest (US-MMS 2017, Table 3) (a) LAI (m^2 m^{-2}) modelled (Eq. 3) and from MODIS (Myneni et al. 2015) with values of $T_{BaseSDD}$, $T_{BaseGDD}$, LAI$_{min}$ and LAI$_{max}$; and (b) T_d (Eq. 4). Vertical lines (5 days apart) give GDD (red) and SDD (blue) values (°C) relative to $T_{BaseGDD}$ (solid) and $T_{BaseSDD}$ (dashed) (horizontal purple lines, °C). Notation is given in Table 1.

https://doi.org/10.5194/gmd-2020-148
Preprint. Discussion started: 17 July 2020

Geoscientific Model Development
Discussions

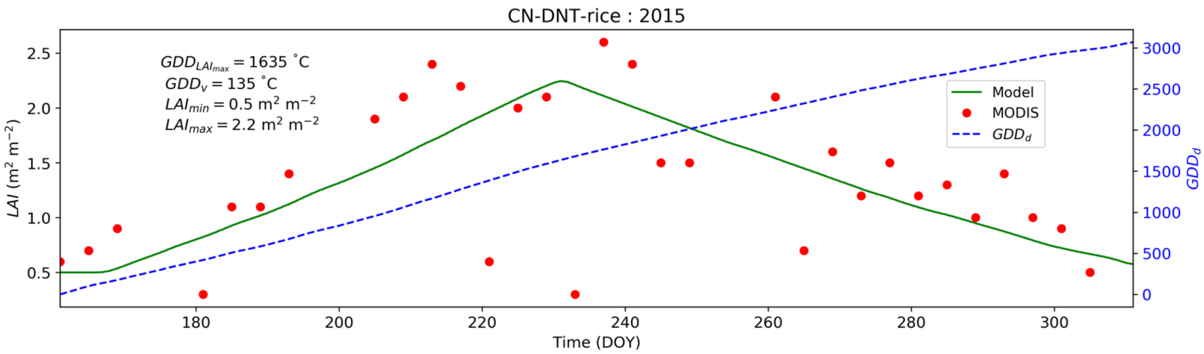

Figure 5: Rice field (CN-DNT-2015 from June 10 (planting) to November 7 (harvest)) LAI: modelled (Eq. 5) and MODIS (Myneni et al. 2015) with values of $GDD_{LAI_{max}}$ (°C), $GDD_{LAI_{min}}$(°C), LAI_{min} (m^2 m^{-2}) and LAI_{max} (m^2 m^{-2}); and GDD_d (right axis, °C). Notation is given in Table 1.

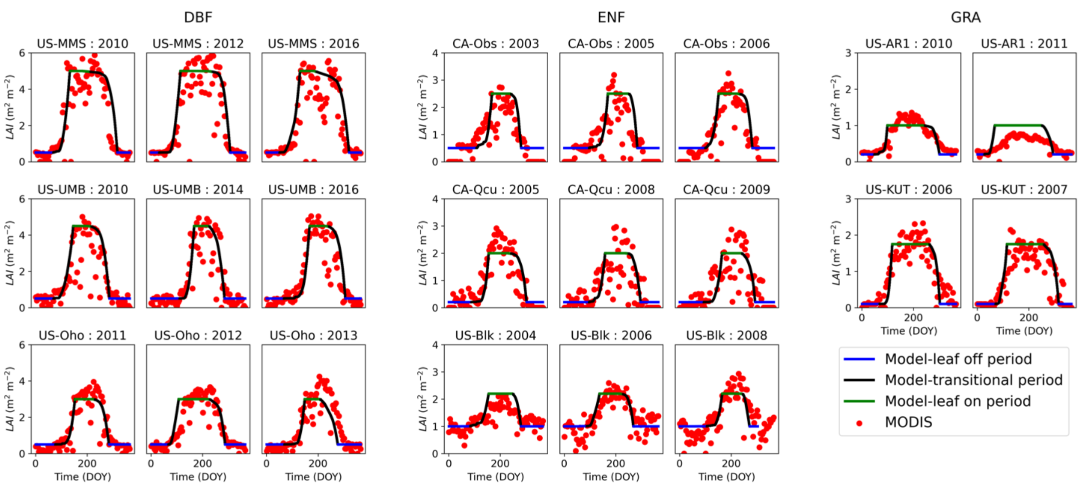

Figure 6: Comparison of LAI (m^2 m^{-2}) calculated (lines, Eq. 3, Table 4 parameters) and MODIS (dots, Myneni et al. *2015) for deciduous (DBF), evergreen (ENF) and grass (GRA) sites (Table 3, Fig.3) for different years with* modelled maxima (green), leaf off (blue), and transitional growth/senescence (black) periods shown.

https://doi.org/10.5194/gmd-2020-148
Preprint. Discussion started: 17 July 2020

Geoscientific Model Development
Discussions
Open Access
EGU

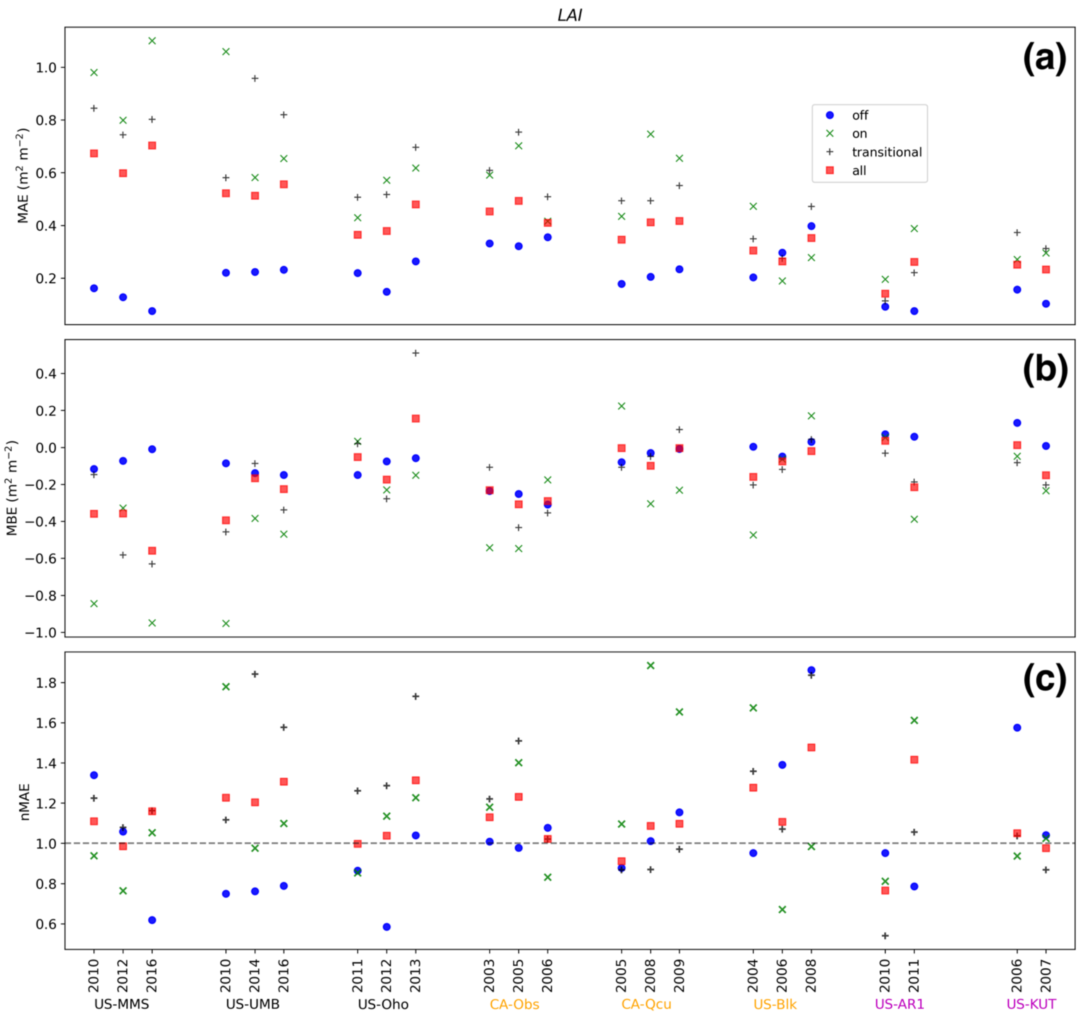

374

375 *Figure 7: Modelled LAI (Eq. 3, Table 4 parameters) evaluated using MODIS (Myneni et al., 2015) for*
376 *entire year (all), leaf on period (maxima), leaf off period (minima), and transitional period*
377 *(growth/senescence period) for DBF (black x-axis label), ENF (yellow) and GRA (purple) sites.*
378 *Performance metrics (Sect. 2.4)* ***a****: MAE* ***b****: MBE* ***c****: nMAE (Sect. 2.4)*

https://doi.org/10.5194/gmd-2020-148
Preprint. Discussion started: 17 July 2020

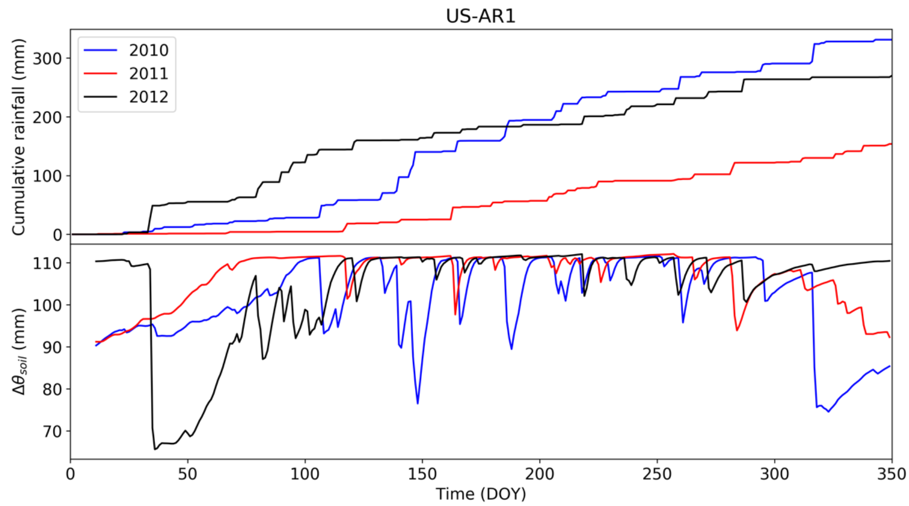

Figure 8: Grassland site (US-AR1) (a) cumulative rain and (b) SUEWS modelled soil moisture deficit ($\Delta\theta_{soil}$) for three years: 2012 (calibration), 2010 and 2011 (test years). SUEWS spun up for each year using the same year data until the soil moisture deficit converges.

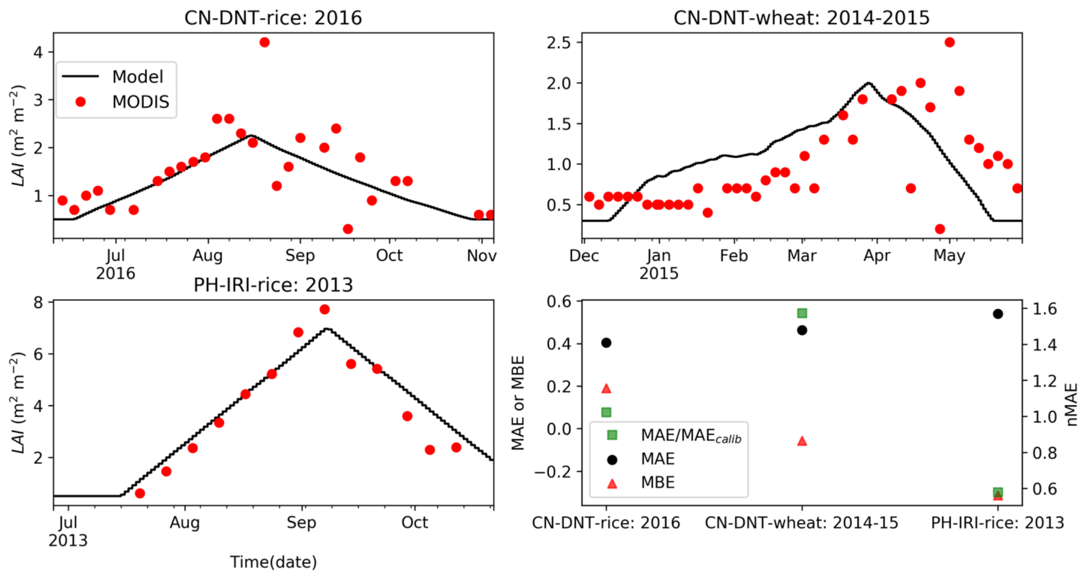

*Figure 9: Crop site (Table 3) LAI (m^2 m^{-2}) results **a-c**: using Eq. 5 with Table 4 parameters (lines) and MODIS (dots, Myneni* et al., *2015) by time and site (Table 3, Fig.3); and **d:** evaluation statistics (Sect. 2.4).*

https://doi.org/10.5194/gmd-2020-148
Preprint. Discussion started: 17 July 2020

Geoscientific Model Development
Discussions

*Table 4: Parameters derived for LAI using Eq. 3 (DBF, ENF, GRA) and Eq. 5 (RIC, WHT) and albedo (Eq. 6). Bare soil (BSV) $\alpha_{LAI_{min}}$ is derived from the first 4 weeks of CN-DNT-rice. Water (WAT) is only for JP-SWL. Crop site air temperature at planting (T_{plant}) * is the 5 day mean.*

Site	*Cover*	LAI_{min}	LAI_{max}	$T_{BaseSDD}$	$T_{BaseGDD}$		$\alpha_{LAI_{min}}$	$\alpha_{LAI_{max}}$
		m^2 m^{-2}	m^2 m^{-2}	°C	°C		-	-
US-MMS	DBF	0.5	5.0	21	8		0.10	0.14
US-UMB	DBF	0.5	4.5	20	6		0.10	0.14
US-Oho	DBF	0.5	3.0	21	8		0.10	0.14
CA-Obs	ENF	0.5	2.5	15.0	5		0.08	0.07
CA-Qcu	ENF	0.2	2.0	11	2		0.08	0.15
US-Blk	ENF	1.0	2.2	16	5		0.08	0.07
US-AR1	GRA	0.2	1.0	20	5		0.14	0.19
US-KUT	GRA	0.1	1.7	13	3		0.18	0.21
				T_{plant}	GDD_v	$GDD_{LAI_{max}}$		
				°C	°C	°C		
CN-DNT	RIC	0.5	2.25	22.5*	135	1635	0.10	0.17
CN-DNT	WHT	0.3	2.0	9.0*	90	770	0.12	0.18
PH-IRI	RIC	0.5	7	29.0*	475	1970	0.09	0.18
JP-SWL	WAT	-	-	-	-	-	0.05	-
CN-DNT	BSV	-	-	-	-	-	0.10	-

3.2 Albedo parameters

The daily albedo simulated with Eq. 6 (Table 4 parameters) clearly shows similar intra-annual evolution as the observations (Fig. 10, 11, snow-free periods, α< 0.3). Some sites (e.g. CA-Qcu) have an α ~ 0.85 during snow. Although the snow flags (Sect. 2.1.2) do not identify all snow days (i.e. high albedo), they approximately indicate snow periods.

As our sites are snow-free between May and October (Fig. 10, F1), the independent evaluations use this period (except for crops). The crops are evaluated between planting and harvest (Fig. 11). Overall, the modelled and observed albedos are in good agreement (Fig. 12, Table D2) during the snow-free periods (May-October for AmeriFlux sites, and entire period for other sites) with $\mathrm{MAE} < 0.025$, $-0.012 < \mathrm{MBE} < 0.025$ and $0.5 < \mathrm{nMAE} < 1.6$ (Fig. 12). Water (0.05) and bare soil (0.10) albedo are treated as constants (Table 4, consistent with Gascoin et al. (2009) and Nunez et al. (1972)).

https://doi.org/10.5194/gmd-2020-148
Preprint. Discussion started: 17 July 2020

Geoscientific Model Development
Discussions
Open Access
EGU

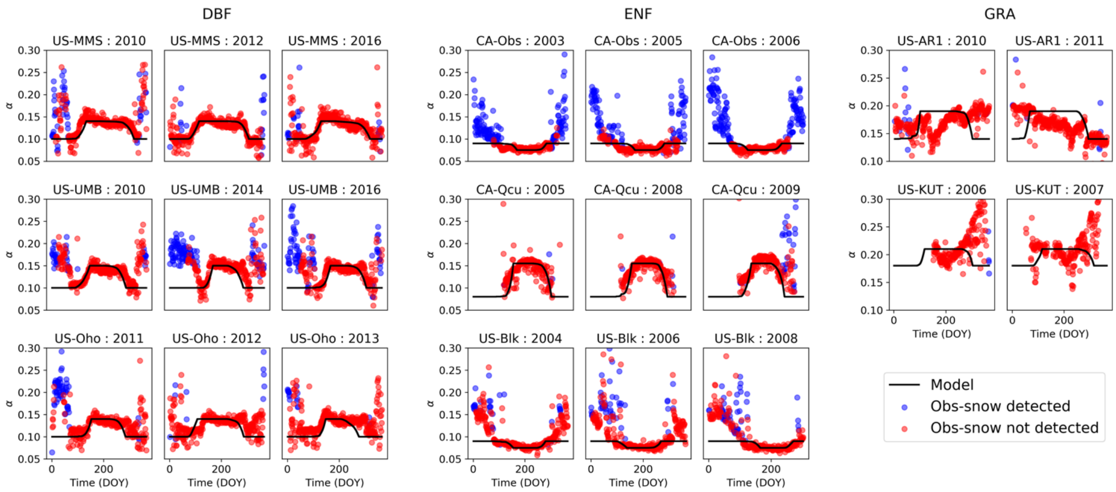

Figure 10: Modelled (Eq. 6, lines) and observed (Sect. 2.1.2) daily albedo by time (day of year, red – snow free, blue - snow-covered, Sect. 2.3) for different vegetation types (Table 3). Note y-axis (albedo) varies between vegetation types.

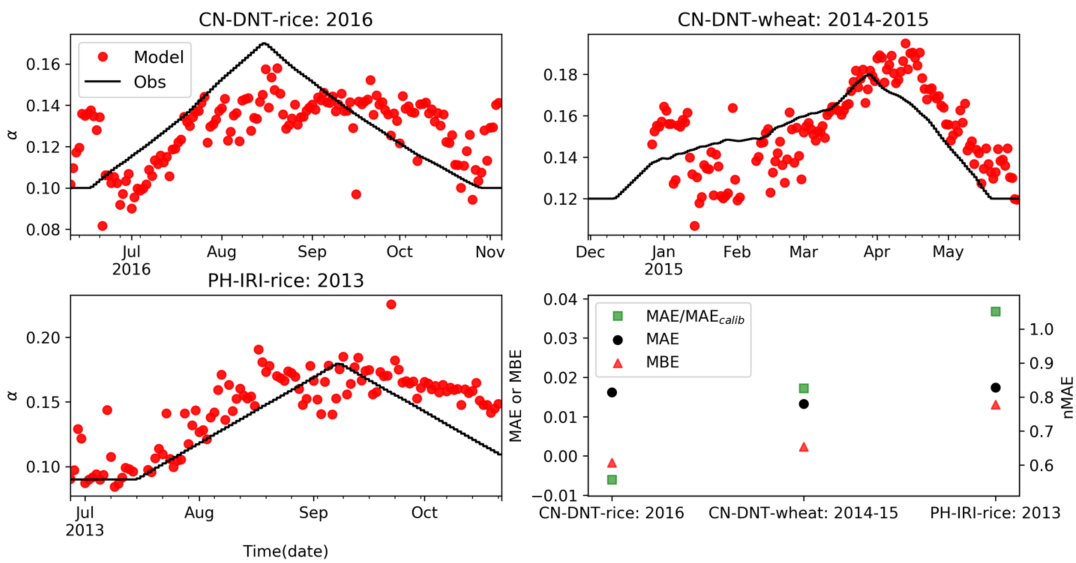

*Figure 11: Daily crop albedo **a-c:** modelled (Eq. 6 with Table 4 parameters, lines) with observations by time (date) for three cases (Table 3), and **d**: evaluation statistics.*

https://doi.org/10.5194/gmd-2020-148
Preprint. Discussion started: 17 July 2020

Geoscientific Model Development
Discussions
Open Access

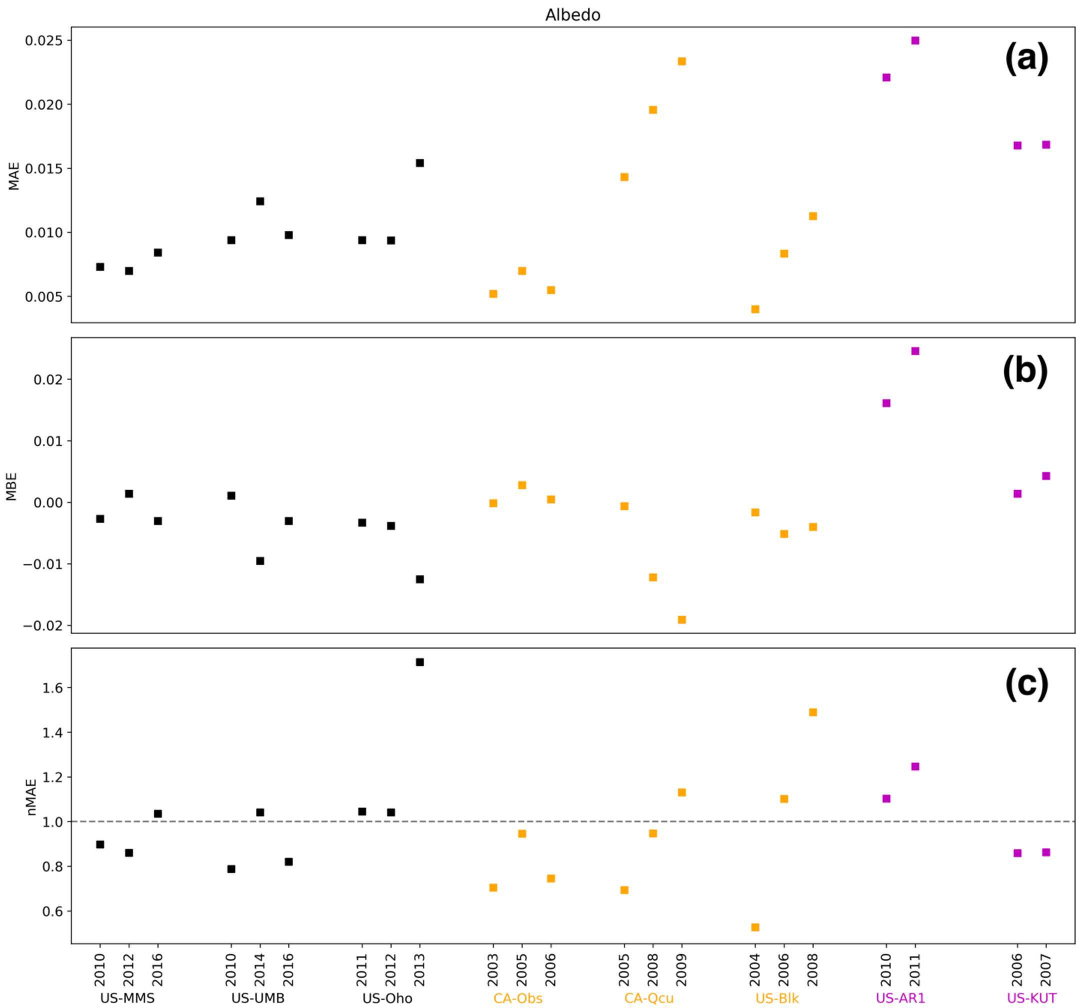

Figure 12: As Fig. 7, but for albedo assessed during a snow free period (May- October).

3.3 Surface conductance parameters

To model Q_E, $g_{\max}$ and $[G_2 - G_6]$ are essential (Sect. 2.1.4). Here observed $K_{\downarrow}$, T_a, Δq and modelled LAI (Fig. 2, 3) and $\Delta\theta_{soil}$ are used when fitting the parameters (Table 5). The values obtained for different pervious land cover types are summarised in Table 5. G_2 (related to $K_{\downarrow}$), G_5 (related to T_a) and G_4 (related to Δq) do not vary substantially among different land types. G_6 (related to $\Delta\theta_{soil}$) is quite similar for DBF, ENF and GRA but varies for other land cover types. However, $g_{\max}$ varies between all the land cover types.

https://doi.org/10.5194/gmd-2020-148
Preprint. Discussion started: 17 July 2020

Geoscientific Model Development Discussions
Open Access
EGU

Using the derived parameters (Table 5), the SUEWS ability to predict Q_E is assessed across the test sites and years (Fig. 13, 14; Table D3). In general, for the DBF, ENF and GRA sites the MAE (for all *LAI* states) is less than 58.5 W m^{-2} (Table D3) with a slight overestimation for most of the sites in the leaf-on period (e.g. US-MMS, CA-Obs, CA-Qcu; MBE: 8.8 to 40.4 W m^{-2}; Fig. 14, Table D3). Q_E is overestimated in the leaf-transitional period at US-AR1 (MBE = 8.1 W m^{-2}) and underestimated at US-KUT (MBE = –18.2 W m^{-2}). For CRP, WAT and BSV, the MAE of Q_E is generally less than 44.5 W m^{-2}. For WAT, the smaller nocturnal overestimation of Q_E may result from overestimation of nocturnal storage heat flux.

Multiple factors influence the Q_E performance: over/under estimation of *LAI* (modifying albedo and conductance) at vegetated sites; over/under prediction of storage heat flux (from for example, missing moisture feedbacks); and/or assuming homogeneous fetch around each site.

Compared with using urban specific parameters, such as those derived for London and Swindon, Ward *et al.,* 2016), those derived for non-urban land covers (Table 5) improve SUEWS Q_E performance (Appendix E): MAE is reduced (cf. MAE_{Ward}) and nMAE is less than one for all the sites (Fig. E2).

Table 5: Surface conductance (Eq. 13-16) parameters (sites, Fig. 3) derived for different land cover types. Note individual site values are not reported.

Land cover	g_{max} (m s^{-1})	G_2 (W m^{-2})	G_3	G_4	G_5 (°C)	G_6 (mm^{-1})
DBF	89.9	104.10	0.16	0.57	25.92	0.028
ENF	14.9	104.64	0.70	0.63	36.62	0.022
GRA	24.2	104.85	0.49	0.61	36.63	0.022
RIC	234.8	105.13	0.97	0.75	36.91	0.046
WHT	747.5	104.45	0.16	0.70	37.37	0.048
BSV	10.9	108.93	0.93	0.96	42.26	0.041

https://doi.org/10.5194/gmd-2020-148
Preprint. Discussion started: 17 July 2020

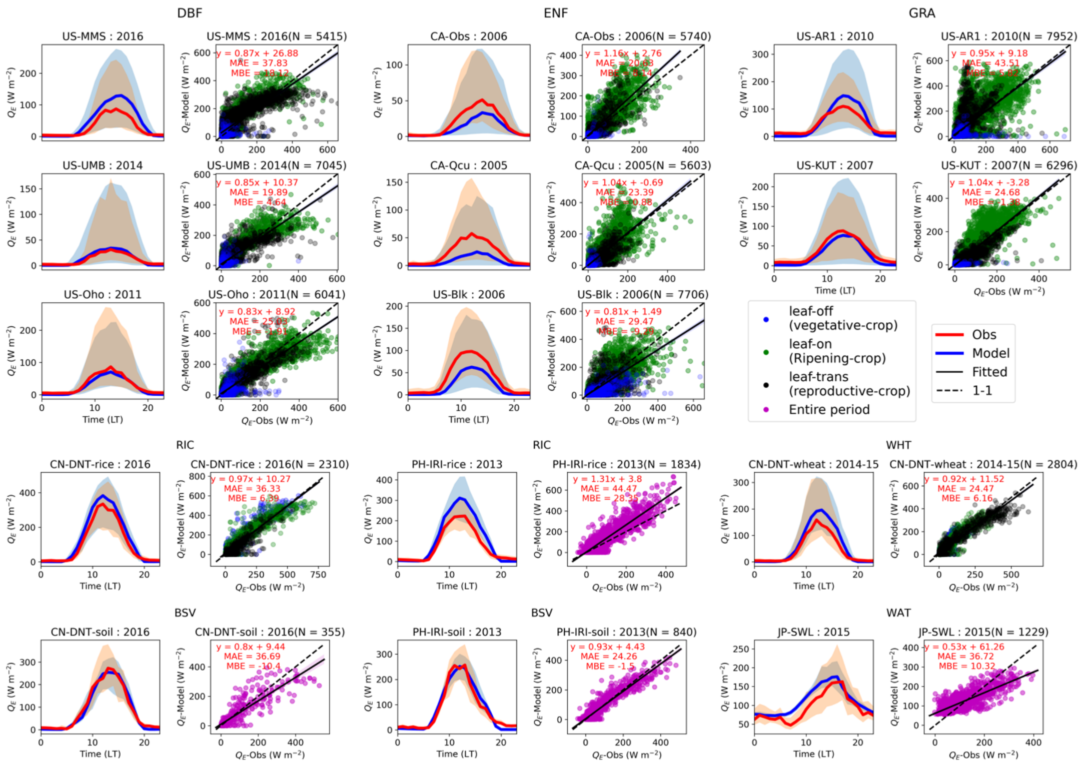

Figure 13: Latent heat flux for different sites (Table 3) calculated by SUEWS (Eq. 8 with Table 5 parameters) with annual diurnal pattern (median (lines) and interquartile range (shading)) for observed (red) and model (blue)) and scatter (dots, colour for LAI period, and N is the number of data points). Note for water and flood period for rice, r_s in Eq. 12 is zero and potential evaporation is calculated.

https://doi.org/10.5194/gmd-2020-148
Preprint. Discussion started: 17 July 2020

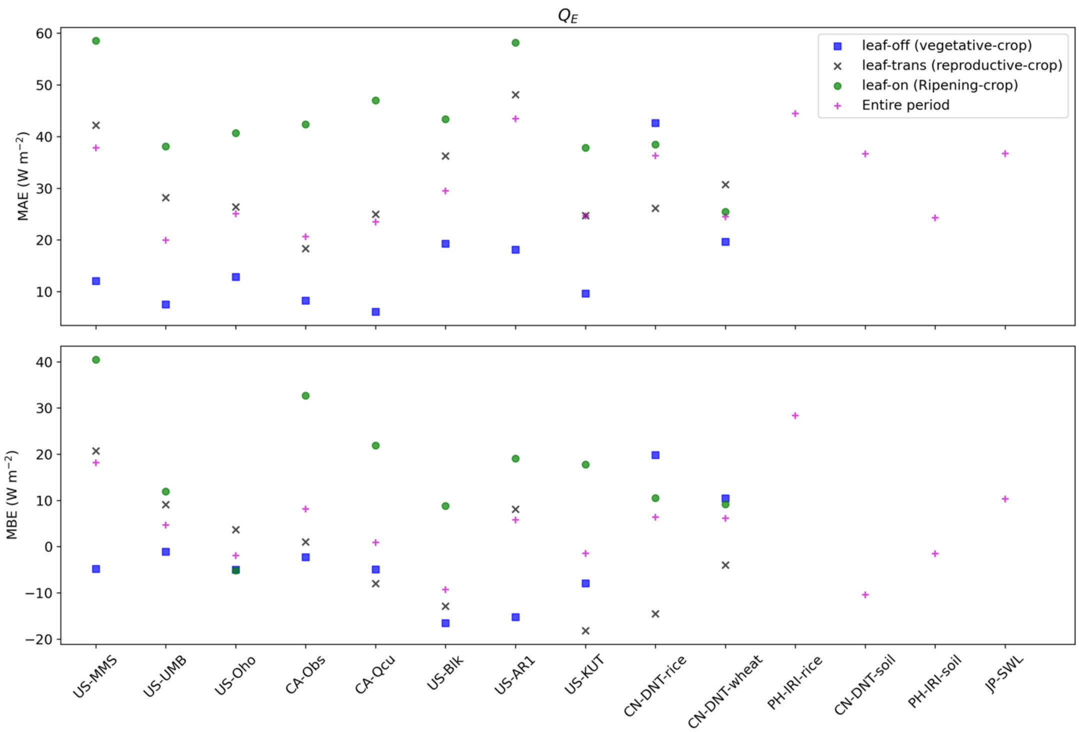

Figure 14: As Fig. 7, but for Q_E (Eq. 8, Table 5 parameters). Units W m^{-2}

4 Concluding remarks

New SUEWS parameters to simulate *LAI*, albedo and latent heat flux for different extensive pervious (i.e. non-urban) land covers are derived and independently evaluated. The Python Jupyter Notebooks protocol to derive the parameters is provided (Fig. 2, GitHub repository in Omidvar *et al.,* 2020). This can be applied to other sites (or to other time periods at these sites). The order of parameter determination is critical (*LAI* → albedo → surface resistance/ conductance, Fig 2, 3) to ensure appropriate values are obtained.

Recommended values are given in Table 6 based on the variability of different parameters derived in this paper. In agreement with previous studies (e.g. Bobée *et al.,* 2012), we find that soil moisture impacts *LAI* for vegetation with shallow roots (e.g. grass). This feedback should be considered in future LAI modelling for SUEWS.

Using the derived (Table 2, 4, 5, 6) parameters or obtaining new values from the protocol (Omidvar *et al.,* 2020) gives broader applicability of SUEWS in non-urban areas and thus

https://doi.org/10.5194/gmd-2020-148
Preprint. Discussion started: 17 July 2020

improves the model performance (cf. SUEWS runs using urban specific resistances, assuming f_i= 1). Use of these derived parameters in online SUEWS applications should improve representation of land-atmosphere interactions.

Table 6: Recommended values for SUEWS parameters (Table 1) for pervious land cover where ranges in *LAI*, albedo and roughness parameters indicate regional variations.

Cover		DBF	ENF	GRA	RIC	WHT	BSV	WAT
LAI(Table 4)								
LAI_{min}	$m^2\ m^{-2}$	0.5	0.2-1.0	0.2-1.0	0.5	0.2	-	-
LAI_{max}	$m^2\ m^{-2}$	3.0-5.0	2.0-2.5	1.0-1.7	1.7-7.0	2.0	-	-
T_{BaseSD}	°C	20-21	11-16	13-20	-	-	-	-
T_{BaseGD}	°C	6-8	2-5	3-5	-	-	-	-
GDD_v	°C	-	-	-	135-475	90	-	-
GDD_{LA}	°C	-	-	-	1635-1970	770	-	-
Albedo(Table 4)								
$\alpha_{LAI_{min}}$	-	0.1	0.8	0.14-0.18	0.09-0.10	0.12	0.1	0.05
$\alpha_{LAI_{max}}$	-	0.14	0.07-0.15	0.19-0.21	0.17-0.18	0.18	-	-
Surface conductance(Table 5)								
g_{max}	$m\ s^{-1}$	33.5	21.8	13.8	276.8	660.8	10.9	-
G_2	$W\ m^{-2}$	104.82	104.38	104.47	104.71	105.08	108.93	-
G_3	-	0.53	0.51	0.79	0.19	0.17	0.93	-
G_4	-	0.61	0.77	0.59	0.57	0.68	0.96	-
G_5	°C	36.3	36.28	37.24	36.46	36.76	42.26	-
G_6	mm^{-1}	0.03	0.023	0.025	0.049	0.044	0.041	-
OHM storage heat flux(Table 2)								
a_1	-	0.215	0.215	0.215	0.185	0.283	0.210	0.880
a_2	s	0.325	0.325	0.325	0.615	0.784	0.902	0.370
a_3	$W\ m^{-2}$	-19.9	-19.9	-19.9	-18.0	-18.0	-20.4	-85.4
Canopy water storage capacity(Table 2)								
S_i	mm	1.3	0.8	1.9	1.9	1.9	1.9	-

Aerodynamic roughness (Table B1) by phenological state with f_0 (Eq. B2) and f_d (Eq. B3) parameters

			DBF	ENF	GRA	RIC	WHT	BSV	WAT
z_{0m}	m	Leaf-off/ vegetative | 0.16	3.2-5.2	0.3-5.1	0.01-0.03	0.24	0.12	0.002	0.0005
		Trans./ reproductive| 0.18	3.9-5.5	0.3-2.6	0.01	0.19	0.2		
		Leaf-on/ ripening | 0.18	3.2-5.4	1.8-2.4	0.02-0.03	0.55	0.38		
z_d	m	Leaf-off /vegetative | 0.5	7.2-19.2	3.7-6.5	0.06-0.83	0.32	0.14	0	0
		Trans/ reproductive | 0.44	8.2-15.4	2.2-6.6	0.06-0.9	0.39	0.45		
		Leaf-on/ripening | 0.42	8.0-10.9	3.8-6.6	0.06-0.83	0.88	0.65		

https://doi.org/10.5194/gmd-2020-148
Preprint. Discussion started: 17 July 2020

Geoscientific Model Development
Discussions
Open Access

Appendix A: SUEWS developments included in v2020a

A.1 SUEWS surface temperature (*T_s*) calculation

At each time step, the surface temperature T_s is calculated iteratively. First T_s is estimated by NARP (net-all radiation parameterization) (Offerle *et al.,* 2003; Loridan *et al.,* 2011) as a function of air temperature T_a (i.e., $T_s^{NARP} = NARP(T_a)$), then T_s^{NARP} is used to calculate Q^* (via outgoing longwave radiation $L_\uparrow$). At the end of this iteration (*j*), T_s is updated using sensible heat flux Q_H and T_a based on Monin-Obukhov similarity theory (MOST) to give a new value $T_{s,j}$ (*j*=1, initial iteration). In subsequent iterations, the NARP-based estimation of T_s is skipped and $T_{s,j-1}$ (i.e., previous iteration) is used in the Q^* calculation and updated to $T_{s,j}$ (i.e. current iteration) using MOST. Once $\left|T_{s,j-1} - T_{s,j}\right| <$ a prescribed tolerance, then $T_s = T_{s,j}$ and iteration stops (or for *j*= 20)

A.2 SUEWS irrigation scheme for crops

Automatic irrigation can be set (`WaterUseMethod`=1 in RunControl.nml file) to maintain the water availability at a specified level h_m (e.g. a certain depth of ponding water for flood irrigation of rice or a particular soil moisture state of other crops; by setting column h_m of SUEWS_Irrigation.txt file, in mm). When it is a positive value it allows for flood irrigation (e.g. rice); otherwise, the soil moisture is maintained by irrigation at the maximum soil storage capacity minus h_m. The running water balance considering precipitation, irrigation, evaporation and runoff rates and the net change in storage is used to determine the irrigation needed (cf. Eq. 2) taking h_m in to account. The irrigation needed (I_N) is determined at the last time step of the day. The I_e water is applied the next day if needed (i.e. for I_N > 0 mm) based on the rates specified by the user via the SUEWS automatic irrigation profile f_a. The automatic irrigation profile allows water to be supplied at the appropriate times of the day and intensity for the region. If the water is applied too rapidly (e.g. all in one 5 min timestep) unrealistic runoff will occur. At each time step, the I_N is checked to confirm that water is still needed (as determined by I_N at the end of the previous day). If there is need remaining at the end of the day this will be included in the end of day water balance calculation for the next day.

A.3 SUEWS land cover adaptive z_{0v} scheme

A new option RoughLenHeatMethod (choice 5) is included (RunControl.nml) that allows different z_{0v} schemes to be used depending on the land cover characteristics. If no impervious cover exists in a grid (f_{prv} = 1) then Brutsaert's (1982) method is used:

https://doi.org/10.5194/gmd-2020-148
Preprint. Discussion started: 17 July 2020

Geoscientific Model Development
Discussions
Open Access

$$z_{0v} = 0.1 z_{0m} \tag{A1}$$

Otherwise (f_{prv} <1) Kawai *et al.* (2009) is used:

$$z_{0v} = z_{0m} \exp\left(2 - \left(1.2 - 0.9 f_{prv}^{0.29}\right)\left(\frac{u_* z_{0m}}{\mu}\right)^{0.25}\right) \tag{A2}$$

where z_{0m} is the roughness length for momentum, u_* the friction velocity, and μ the molecular diffusivity of air.

Appendix B: Roughness length and zero-displacement height for momentum

B.1 Methods

The roughness parameters (z_{0m}, z_d) are derived during neutral stability ($|(z_m - 0.7h_v)/L)| < 0.01$, i.e. assuming initially z_d=$0.7h_v$) using observed u_* and u (Monin and Obukhov, 1954):

$$u = \frac{u_*}{\kappa} \ln\left[\frac{z_m - z_d}{z_{0m}}\right] \tag{B1}$$

These can also be obtained simply using a rule of thumb (Garratt 1991, Grimmond and Oke 1999):

$$z_{0,m} = f_{0,i} h_{v,i} \tag{B2}$$

$$z_d = f_{d,i} h_{v,i} \tag{B3}$$

where h_{vi} *is the vegetation height for type i and* $f_{0,i}$ and $f_{d,i}$ depend on porosity of the vegetation type.

The same multi-objective evolutionary algorithm used to determine G_2 - G_6 (Sect. 2.1.4), is applied with two objectives to optimize Eq. B1: (1) to minimize the normalized (n) standard deviation (SD) of observations (obs) *of u*:

$$\text{nSD} = \frac{SD(u_{mod}) - \text{SD}(u_{obs})}{SD(u_{obs})} \tag{B4}$$

(2) to minimize the *MAE of u (Eq. 22).*

As *LAI* state changes both z_{0m} *and* z_d (e.g. Kent et al. 2017b) by modifying the porosity of the canopy, the three phenological states (leaf off, on and transition, Sect. 3.1) are considered. However, sufficient data (> 20, Grimmond et al. 1998) need to be used. By undertaking analysis by wind direction for sites that appeared to have variable results (based on modelled *u*) it is also possible to identify sites that have varying fetch by wind direction (e.g. CA-Qcu). This can be

https://doi.org/10.5194/gmd-2020-148
Preprint. Discussion started: 17 July 2020

Geoscientific Model Development Discussions
Open Access
EGU

confirmed using visible wavelength satellite imagery. As CA-Qcu's fetch is found to vary, data are analysed with 10° direction bins (for each *LAI* state) with the median z_{0m} and z_d used.

To obtain the parameters $f_{0,i}$ and $f_{d,i}$ (Eq. B2 and B3) vegetation heights are needed (Table 3). As crop height varies substantially through a season, where heights are available (e.g. C-DNT, Duan *et al.* 2020) these are used. However, for others only one height is used and z_{0m}, z_d are calculated for the entire growth period (e.g. PH-IRI). The training years (Table 3) are used to derive z_{0m}, z_d and subsequently $f_{0,i}$ and $f_{d,I}$.

B.2 Results

Analysis of 'observed' z_{0m} and z_d (*Eq.* B1*)* with height suggests f_0 and f_d (Eq. B2) vary between 0.16 - 0.18 and 0.42-0.5 (Fig. B.1) across phenological states. These values for each *LAI* state are used to derive z_{0m}, z_d of test sites.

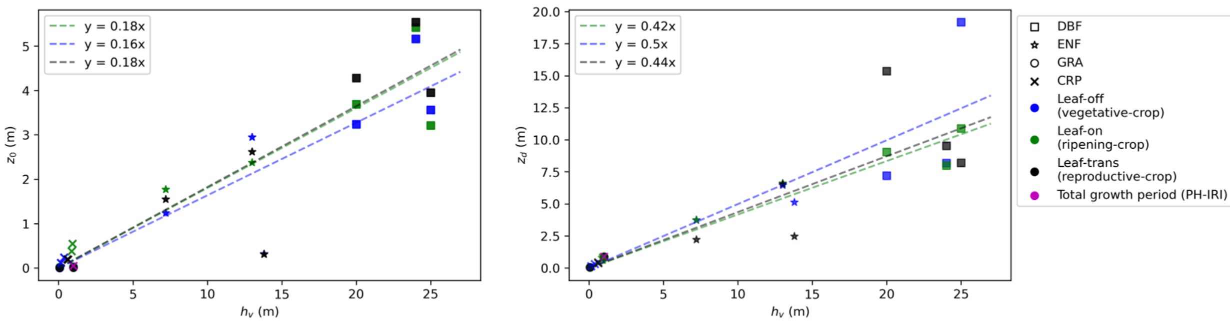

Figure B1: Micrometeorologically derived (Eq. B1) aerodynamic roughness parameters and vegetation height (*Table 3) calculated for* the *calibration years by phenological state (Sect. 3.1)*: *(**a**) z_{0m} and (**b**)* z_d. The crop states heights vary for CN-DNT (Duan et al. 2020) [rice: vegetative =0.39 m, reproductive=0.64 m, ripening=0.93 m; wheat: vegetative=0.15 m, reproductive = 0.58 m ripening=0.86 m] but not for Ph-IRI.

The ability to predict *u is assessed* for different sites with LAI/crop state using Eq. B1 and the derived z_{0m} and z_d values (Table B1). These are in generally good agreement with observations (Fig. B2), with MAE < 1.32 m s^{-1} and -1.03 < MBE <1.22 m s^{-1}.

https://doi.org/10.5194/gmd-2020-148
Preprint. Discussion started: 17 July 2020

Geoscientific Model Development Discussions Open Access EGU

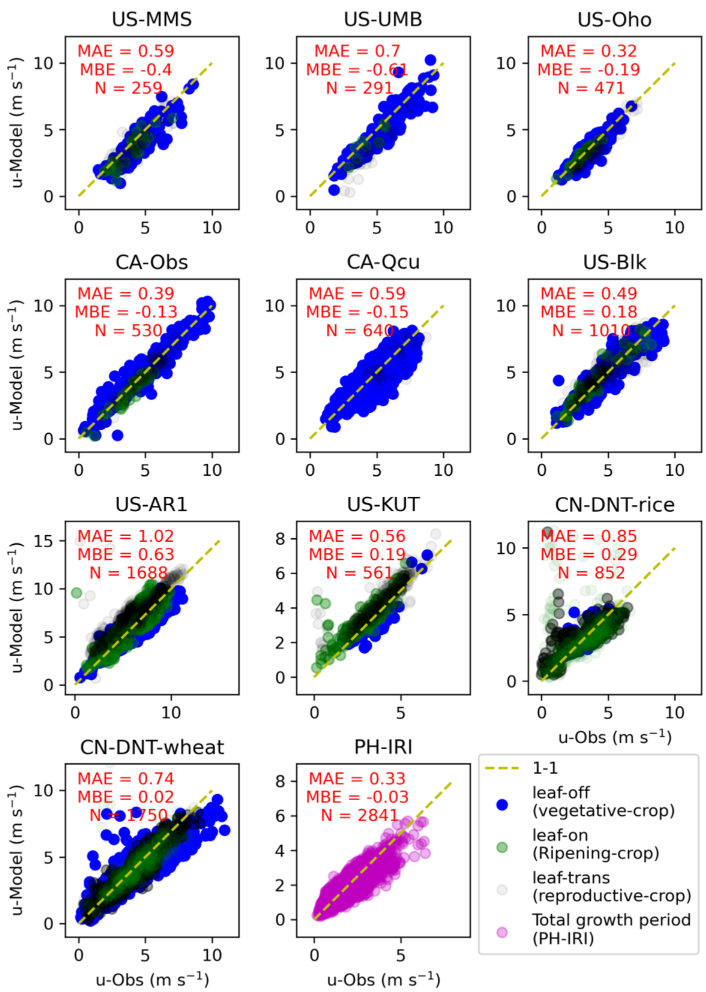

Figure B2: Comparison of observed u (u-Obs) to modelled u (u-Model, z_{0m} and z_d Eq. B1, Table B1) at the vegetated sites for all training years (Table 3) with number (N) data points and phenology (Sect. 3.1) and CN-DNT crop states (Duan et al. 2020).

Table B1: Micrometeorological (Eq. B1) z_{0m} and z_d for vegetation sites (Table 3) for number (N) data points for different phenology periods (Sect. 3.1) and for CN-DNT crop states (Duan et al. 2020). MAE (m s^{-1}) and MBE (m s^{-1}) are calculated for u.

	Leaf-off					**Leaf-trans**					**Leaf-on**				
site	z_{0m} (m)	z_d (m)	*MAE*	*MBE*	*N*	z_{0m} (m)	z_d (m)	*MAE*	*MBE*	*N*	z_{0m} (m)	z_d (m)	*MAE*	*MBE*	*N*
US-MMS	3.56	19.19	0.58	-0.38	145	3.95	8.2	0.66	-0.40	89	3.21	10.9	0.54	-0.41	25
US-UMB	3.24	7.22	0.58	-0.44	221	4.28	15.36	1.03	-1.03	48	3.69	9.06	0.50	-0.36	22
US-Oho	5.16	8.18	0.33	-0.19	354	5.54	9.54	0.46	-0.38	90	5.42	7.99	0.16	0.0	27
CA-Obs	1.24	3.73	0.41	0.12	371	1.55	2.22	0.39	-0.16	124	1.77	3.76	0.39	-0.36	35
CA-Qcu	0.32	5.14	0.58	-0.14	602	0.31	2.47	0.72	-0.16	38	-	-	-		-
US-Blk	2.95	6.46	0.45	0.12	727	2.62	6.56	0.58	0.22	230	2.38	6.63	0.44	0.20	53
US-AR1	0.03	0.83	0.82	0.28	938	0.01	0.9	1.32	1.22	442	0.03	0.83	0.91	0.38	308

https://doi.org/10.5194/gmd-2020-148
Preprint. Discussion started: 17 July 2020

US-KUT	0.01	0.06	0.59	-0.38	54	0.01	0.06	0.57	0.52	330	0.02	0.06	0.5	0.43	177
	Vegetative-crop					**Reproductive-crop**					**Ripening-crop**				
CN-DNT-rice	0.24	0.32	0.42	0.05	112	0.19	0.39	0.84	0.26	318	0.55	0.88	1.30	0.55	422
CN-DNT-wheat	0.12	0.14	0.91	0.02	754	0.2	0.45	0.48	-0.14	575	0.38	0.65	0.85	0.19	421
	Total Growth Period														
PH-IRI-rice	0.05	0.89	0.33	-0.03	2841										

Appendix C: Latent heat flux (Q_E) in extremely cold conditions

As the surface conductance (Eq. 12) has an air temperature dependency with limits (i.e. T_L in Eq. 15), we investigate the T_L limit with Q_E below -10°C for different sites (Fig. C1). Given this we use T_L = –20°C for all sites as the limit when evaporation switches off in SUEWS.

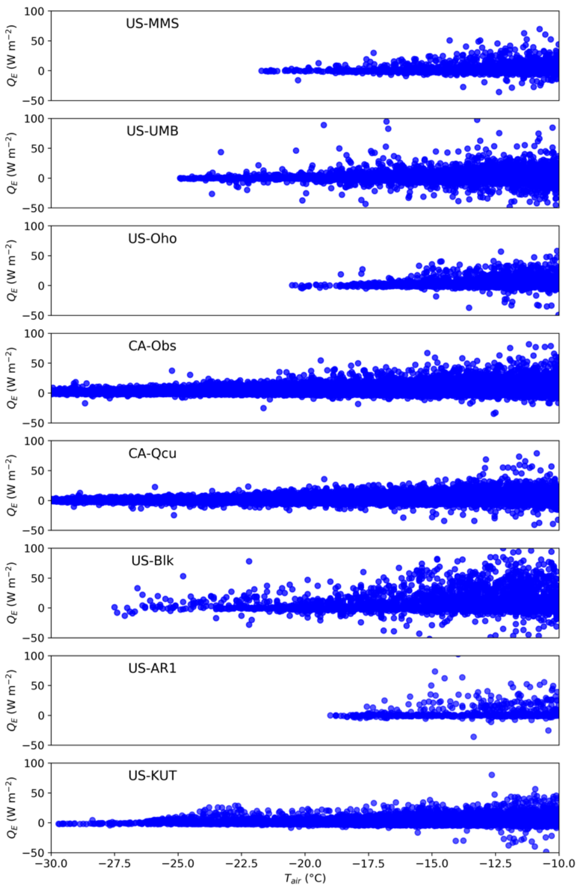

Figure C1: Latent heat flux Q_E variation with air temperature T_a when T_a < –10°C at eight sites (Table 3).

https://doi.org/10.5194/gmd-2020-148
Preprint. Discussion started: 17 July 2020

Appendix D: *Model evaluation statistics*

Sites (Table 3) used to evaluated (metrics Sect. 2.4) the parameters assessed LAI (Table D1), albedo (Table D2) and latent heat flux (Table D3).

Table D1: Evaluation of SUEWS modelled LAI (Eq. 3 or 5, with parameters Table 4) and MODIS LAI product (Myneni et al., 2015) for entire year (all), leaf on period (model LAI - maxima), leaf off period (LAI model - minima), and transitional period (growth/senescence period).Units: m^2 m^{-2}. N is the number of data points in each period for each site

site	year	All			Leaf-off			Transitional			Leaf-on		
		MAE	MBE	N	MAE	MBE	N	MAE	MBE	N	MAE	MBE	N
US-MMS	2010	0.67	−0.36	94	0.16	−0.12	30	0.84	−0.15	44	0.98	−0.84	20
	2012	0.60	−0.36	92	0.12	−0.05	23	0.88	−0.70	38	0.80	−0.33	31
	2016	0.70	−0.56	91	0.08	−0.01	24	0.80	−0.63	51	1.10	−0.95	16
US-UMB	2010	0.52	−0.39	92	0.22	−0.09	38	0.58	−0.46	36	1.06	−0.95	18
	2014	0.51	−0.17	92	0.22	−0.14	48	0.96	−0.09	29	0.58	−0.38	15
	2016	0.56	−0.23	90	0.23	−0.15	30	0.82	−0.34	41	0.65	−0.47	19
US-Oho	2011	0.36	−0.05	94	0.22	−0.15	40	0.51	0.02	34	0.43	0.03	20
	2012	0.38	−0.17	93	0.15	−0.08	37	0.52	−0.28	25	0.57	−0.23	31
	2013	0.48	0.16	93	0.24	−0.04	40	0.74	0.54	37	0.62	−0.15	16
CA-Obs	2003	0.45	−0.23	91	0.33	−0.24	47	0.61	−0.11	25	0.59	−0.54	19
	2005	0.49	−0.31	95	0.32	−0.25	46	0.75	−0.43	28	0.70	−0.55	21
	2006	0.41	−0.29	93	0.35	−0.31	46	0.51	−0.35	25	0.42	−0.17	22
CA-Qcu	2005	0.35	−0.03	92	0.20	−0.13	38	0.48	−0.13	32	0.43	0.22	22
	2008	0.42	−0.13	94	0.23	−0.08	43	0.48	−0.08	38	0.75	−0.31	23
	2009	0.42	−0.04	93	0.26	−0.05	42	0.54	0.07	41	0.66	−0.23	20
US-Blk	2004	0.30	−0.16	93	0.20	0.01	43	0.35	−0.20	26	0.47	−0.47	24
	2006	0.26	−0.07	94	0.30	−0.05	47	0.27	−0.12	24	0.19	−0.06	23
	2008	0.35	−0.02	92	0.40	0.03	51	0.47	0.04	21	0.28	0.17	20
US-AR1	2010	0.13	0.01	94	0.06	0.03	29	0.11	−0.07	28	0.20	0.05	37
	2011	0.21	−0.18	93	0.04	0.01	25	0.21	−0.17	22	0.34	−0.34	46
US-KUT	2006	0.25	0.01	93	0.16	0.13	24	0.37	−0.08	23	0.27	−0.05	36
	2007	0.23	−0.15	92	0.10	0.01	31	0.31	−0.20	25	0.30	−0.23	36
CN-DNT-rice	2016	0.40	0.19	28	-	-	-	-	-		-	-	-
CN-DNT-wheat	2014-15	0.46	-0.06	42	-	-	-	-	-		-	-	-
PH-IRI	2013	0.53	-0.31	13	-	-	-	-	-		-	-	-

Table D2: As Table D1, but albedo (Eq. 6, Table 4) during snow-free periods (May- October; but the entire period for crops).

site	year	MAE	MBE	N
US-MMS	2010	0.007	−0.003	177
	2012	0.007	0.001	183
	2016	0.008	−0.003	182
US-UMB	2010	0.009	−0.001	182
	2014	0.012	−0.010	182
	2016	0.010	−0.003	183
US-Oho	2011	0.009	−0.003	183

https://doi.org/10.5194/gmd-2020-148
Preprint. Discussion started: 17 July 2020

	2012	0.009	−0.004	183
	2013	0.015	−0.012	183
CA-Obs	2003	0.005	−0.000	183
	2005	0.007	−0.003	175
	2006	0.005	−0.000	171
CA-Qcu	2005	0.014	−0.001	180
	2008	0.020	−0.012	180
	2009	0.023	−0.019	183
US-Blk	2004	0.004	−0.002	160
	2006	0.008	−0.005	176
	2008	0.011	−0.004	182
US-AR1	2010	0.022	0.016	183
	2011	0.025	0.025	183
US-KUT	2006	0.017	0.001	145
	2007	0.017	0.004	148
CN-DNT-rice	2016	0.016	-0.001	123
CN-DNT-wheat	2014-15	0.013	0.002	174
PH-IRI	2013	0.017	0.013	113

Table D3: As Table D1, but for Q_E (Eq. 8 with Table 5 parameters). Units: W m^{-2}

		Leaf-off			Leaf-trans			Leaf-on			All		
site	year	MAE	MBE	N	MAE	MBE	N	MAE	MBE	N	MAE	MBE	N
US-MMS	2016	12.1	-4.8	1330	42.2	20.7	3028	58.5	40.4	1057	37.8	18.1	5415
US-UMB	2014	7.5	−1.1	3410	28.2	9.1	2347	38.1	11.9	1288	19.9	4.6	7045
US-Oho	2011	12.8	-5.0	2255	26.4	3.7	2198	40.6	−5.2	1588	25.0	-1.9	6041
CA-Obs	2006	8.3	-2.3	2352	18.3	1.0	1844	42.4	32.7	1544	20.6	8.1	5740
CA-Qcu	2005	6.1	−4.9	2134	25.0	-8.0	2007	47.0	21.9	1462	23.4	0.9	5603
US-Blk	2006	19.3	−16.5	3867	36.2	-12.9	1907	43.3	8.8	1938	29.5	-9.3	7709
US-AR1	2010	18.1	−15.2	2338	48.1	8.1	2323	58.2	19.1	3291	43.5	5.8	7952
US-KUT	2007	9.6	-7.9	2059	24.7	-18.2	1899	37.8	17.8	2338	24.6	-1.5	6296
		Vegetative			Reproductive			Ripening					
CN-DNT-rice	2016	42.6	19.8	610	26.1	-14.5	605	38.4	10.5	1095	36.3	6.4	2310
CN-DNT-wheat	2014	19.6	10.4	1153	30.7	-4.0	752	25.4	9.2	899	24.5	6.2	2804
PH-IRI-rice	2013	-	-	-	-	-	-	-	-	-	44.5	28.3	1834
CN-DNT-soil	2016	-	-	-	-	-	-	-	-	-	36.7	-10.4	355
PH-IRI-soil	2013	-	-	-	-	-	-	-	-	-	24.3	-1.5	840
JP-SWL	-	-	-	-	-	-	-	-	-	-	36.7	10.3	1229

Appendix E: Q_E simulated with London and Swindon parameters

To demonstrate the necessity and benefit of using appropriate parameters to estimate Q_E in SUEWS, we compare Q_E simulated at DBF, ENF and GRA pervious sites using Ward *et al.*'s

https://doi.org/10.5194/gmd-2020-148
Preprint. Discussion started: 17 July 2020

(2016) g_{max} and G_2-G_6 parameters (derived for London and Swindon) (Fig. E1) to those derived here (Table 5). In all cases the performance is improved using pervious area surface parameters (e.g. *LAI,* albedo, surface conductance) than using the suburban/urban parameters (assuming f_i=1 of the pervious area) (Fig. E2).

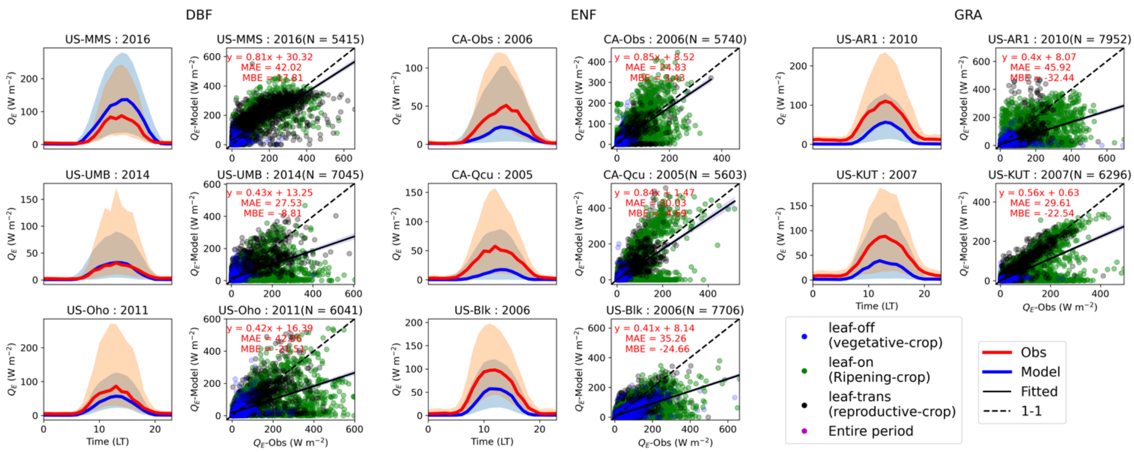

Figure E1: As Fig. 15, but using the parameters from Table A1 in Ward et al. (2016).

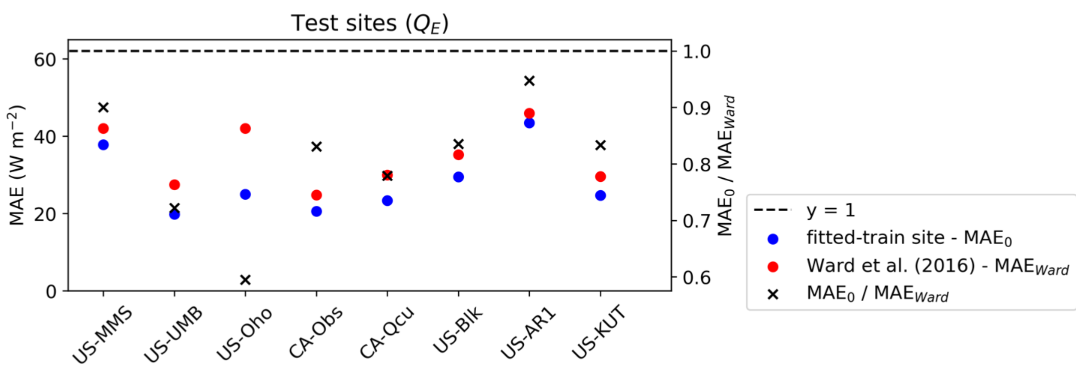

Figure E2: MAE *for* Q_E *(Eq. 5) calculated with site-specific surface conductance parameters for sites (Table 3) (i.e. Table 5,* MAE_0*) and with the Ward et al. (2016) parameters (their Table A1)* (MAE_{W16})*, and the ratio of* MAE_0 *and* MAE_{W16} *for these sites.*

https://doi.org/10.5194/gmd-2020-148
Preprint. Discussion started: 17 July 2020

Geoscientific Model Development
Discussions
Open Access
EGU

Appendix F: *Albedo for May to October period*

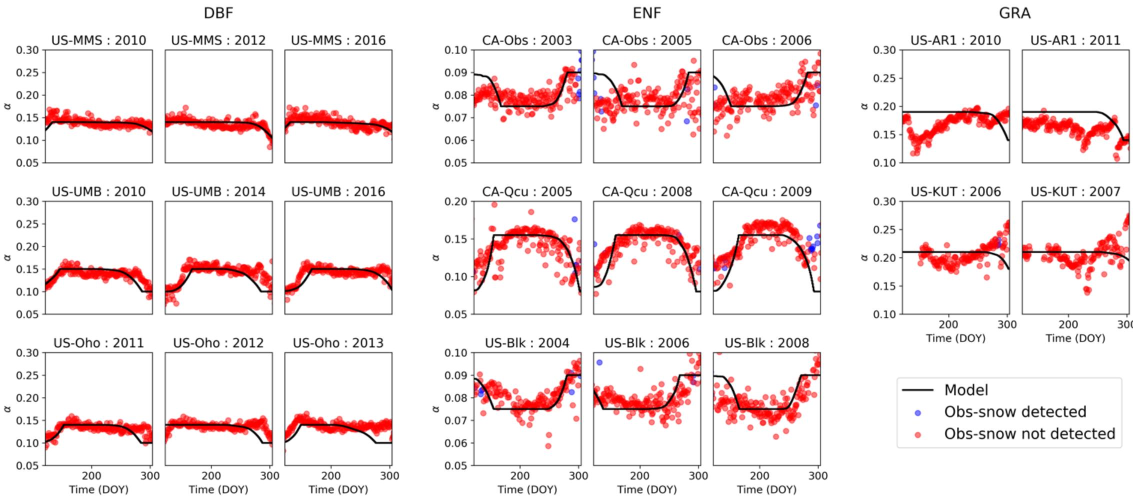

Figure F1: As Fig. 10, but only for May–October period.

Code and data availability

All source codes (Jupyter notebooks and Python scripts), input and output data are archived on Zenodo (https://doi.org/10.5281/zenodo.3831233, Omidvar et al., 2020)

Author contribution

HO, TS and SG contributed to data preparation, model development, running simulations and writing the paper. All other authors (DB, AB, JC, ZD, HI, and JM) provided data, interpreted the results, and reviewed the manuscript.

Competing interest

The authors declare that they have no conflict of interest.

Acknowledgments

This work is funded by NERC-COSMA project (NE/S005889/1), Newton Fund Met Office CSSP-China (SG), NERC Independent Research Fellowship (NE/P018637/1), National Natural Science Foundation of China (41875013; Zhiqiu Gao and Zexia Duan). We thank PIs for providing the data: Kim Novick and Rich Phillips (US-MMS); Christopher Gough, Gil Bohrer and Peter Curtis (US-UMB); Hank A. Margolis (CA-Qcu); Tilden Meyers (US-Blk); James Bradford, Margaret Torn (US-AR1); and Maricar Alberto, Caesar Arloo Centeno, Reiner Wassmann (PH-IRI)

References

Alberto, M. C. R., Wassmann, R., Hirano, T., Miyata, A., Kumar, A., Padre, A. and Amante, M.: CO_2/heat fluxes in rice fields: Comparative assessment of flooded and non-flooded fields in the Philippines, Agric. For. Meteorol., 149(10), 1737–1750, doi:10.1016/j.agrformet.2009.06.003, 2009.

Alemu, W. and Henebry, G.: Characterizing Cropland Phenology in Major Grain Production Areas of Russia, Ukraine, and Kazakhstan by the Synergistic Use of Passive Microwave and Visible to Near Infrared Data, Remote Sens., 8(12), 1016, doi:10.3390/rs8121016, 2016.

Ao, X., Grimmond, C. S. B., Ward, H. C., Gabey, A. M., Tan, J., Yang, X.-Q., Liu, D., Zhi, X., Liu, H. and Zhang, N.: Evaluation of the Surface Urban Energy and Water Balance Scheme (SUEWS) at a Dense Urban Site in Shanghai: Sensitivity to Anthropogenic Heat and Irrigation, J. Hydrometeorol., 19(12), 1983–2005, doi:10.1175/JHM-D-18-0057.1, 2018.

AsiaFlux: AsiaFlux, [online] Available from: www.asiaflux.net (Accessed 22 January 2020), 2003.

Baldocchi, D., Falge, E., Gu, L., Olson, R., Hollinger, D., Running, S., Anthoni, P., Bernhofer, C., Davis, K., Evans, R., Fuentes, J., Goldstein, A., Katul, G., Law, B., Lee, X., Malhi, Y., Meyers, T., Munger, W., Oechel, W., Paw, U. K. T., Pilegaard, K., Schmid, H. P., Valentini, R., Verma, S., Vesala, T., Wilson, K. and Wofsy, S.: FLUXNET: A New Tool to Study the Temporal and Spatial Variability of Ecosystem-Scale Carbon Dioxide, Water Vapor, and Energy Flux Densities, Bull. Am. Meteorol. Soc., 82(11), 2415–2434, doi:10.1175/1520-0477(2001)082<2415:FANTTS>2.3.CO;2, 2001.

Basemap: Basemap Toolkit documentation, [online] Available from: https://matplotlib.org/basemap/ (Accessed 13 February 2020), 2012.

Bauerle, W. L., Oren, R., Way, D. A., Qian, S. S., Stoy, P. C., Thornton, P. E., Bowden, J. D., Hoffman, F. M. and Reynolds, R. F.: Photoperiodic regulation of the seasonal pattern of photosynthetic capacity and the implications for carbon cycling, Proc. Natl. Acad. Sci. U. S. A., 109(22), 8612–8617, doi:10.1073/pnas.1119131109, 2012.

Bergeron, O., Margolis, H. A., Black, T. A., Coursolle, C., Dunn, A. L., Barr, A. G. and Wofsy, S. C.: Comparison of carbon dioxide fluxes over three boreal black spruce forests in Canada, Glob. Chang. Biol., 13(1), 89–107, doi:10.1111/j.1365-2486.2006.01281.x, 2007.

https://doi.org/10.5194/gmd-2020-148
Preprint. Discussion started: 17 July 2020

Geoscientific Model Development
Discussions

Billesbach, D., Bradford, J. and Torn, M.: AmeriFlux US-AR1 ARM USDA UNL OSU Woodward Switchgrass 1, AmeriFlux Netw., doi:10.17190/AMF/1246137, 2009.

Black, T. A.: AmeriFlux CA-Obs Saskatchewan - Western Boreal, Mature Black Spruce, , doi:10.17190/AMF/1375198, 2017.

Bobée, C., Ottlé, C., Maignan, F., De Noblet-Ducoudré, N., Maugis, P., Lézine, A. M. and Ndiaye, M.: Analysis of vegetation seasonality in Sahelian environments using MODIS LAI, in association with land cover and rainfall, J. Arid Environ., 84, 38–50, doi:10.1016/j.jaridenv.2012.03.005, 2012.

Brutsaert, W.: Evaporation into the Atmosphere, Springer Netherlands, Dordrecht., 1982.

Campbell, G. S. and Norman, J. M.: An Introduction to Environmental Biophysics, in An Introduction to Environmental Biophysics, pp. 1–13, Springer New York, New York, NY., 1998.

Chen, J.: AmeriFlux US-Oho Oak Openings, , doi:10.17190/amf/1246089, 2016.

Curtis, P. and Gough, C.: AmeriFlux US-UMB Univ. of Mich. Biological Station, , doi:10.17190/AMF/1246107, 2016.

Curtis, P. S., Hanson, P. J., Bolstad, P., Barford, C., Randolph, J. C., Schmid, H. P. and Wilson, K. B.: Biometric and eddy-covariance based estimates of annual carbon storage in five eastern North American deciduous forests, Agric. For. Meteorol., 113(1–4), 3–19, doi:10.1016/S0168-1923(02)00099-0, 2002.

Doll, D., Ching, J. K. S. and Kaneshiro, J.: Parameterization of subsurface heating for soil and concrete using net radiation data, Boundary-Layer Meteorol., 32(4), 351–372, doi:10.1007/BF00122000, 1985.

Duan, Z., Grimmond, S., Zhiqui, G., Sun, T., Liu, C. and Li, Y.: Radiation, energy, CO2 fluxes and energy balance closure over rice-wheat rotation: diurnal, seasonal and interannual (2014-2017) variations (under review), Agric. For. Meteorol., 2020.

Ek, M. B., Mitchell, K. E., Lin, Y., Rogers, E., Grunmann, P., Koren, V., Gayno, G. and Tarpley, J. D.: Implementation of Noah land surface model advances in the National Centers for Environmental Prediction operational mesoscale Eta model, J. Geophys. Res. Atmos., 108(D22), 2002JD003296, doi:10.1029/2002JD003296, 2003.

Garratt, J.: Review: the atmospheric boundary layer, Earth-Science Rev., 37(1–2), 89–134,

https://doi.org/10.5194/gmd-2020-148
Preprint. Discussion started: 17 July 2020

doi:10.1016/0012-8252(94)90026-4, 1994.

Gascoin, S., Ducharne, A., Ribstein, P., Perroy, E. and Wagnon, P.: Sensitivity of bare soil albedo to surface soil moisture on the moraine of the Zongo glacier (Bolivia), Geophys. Res. Lett., 36(2), n/a-n/a, doi:10.1029/2008GL036377, 2009.

Gill, A. L., Gallinat, A. S., Sanders-DeMott, R., Rigden, A. J., Short Gianotti, D. J., Mantooth, J. A. and Templer, P. H.: Changes in autumn senescence in northern hemisphere deciduous trees: a meta-analysis of autumn phenology studies, Ann. Bot., 116(6), 875–888, doi:10.1093/aob/mcv055, 2015.

Grimmond, C. S. B.: The suburban energy balance: Methodological considerations and results for a mid-latitude west coast city under winter and spring conditions, Int. J. Climatol., 12(5), 481–497, doi:10.1002/joc.3370120506, 1992.

Grimmond, C. S. B. and Oke, T. R.: An evapotranspiration-interception model for urban areas, Water Resour. Res., 27(7), 1739–1755, doi:10.1029/91WR00557, 1991.

Grimmond, C. S. B. and Oke, T. R.: Aerodynamic Properties of Urban Areas Derived from Analysis of Surface Form, J. Appl. Meteorol., 38(9), 1262–1292, doi:10.1175/1520-0450(1999)038<1262:APOUAD>2.0.CO;2, 1999.

Grimmond, C. S. B., Oke, T. R. and Steyn, D. G.: Urban Water Balance: 1. A Model for Daily Totals, Water Resour. Res., 22(10), 1397–1403, doi:10.1029/WR022i010p01397, 1986.

Grimmond, C. S. B., Cleugh, H. A. and Oke, T. R.: An objective urban heat storage model and its comparison with other schemes, Atmos. Environ. Part B. Urban Atmos., 25(3), 311–326, doi:10.1016/0957-1272(91)90003-W, 1991.

Grimmond, C. S. B., King, T. S., Roth, M. and Oke, T. R.: Aerodynamic roughness of urban areas derived from wind observations, Boundary-Layer Meteorol., 89(1), 1–24, doi:10.1023/A:1001525622213, 1998.

Grimmond, C. S. B., Blackett, M., Best, M. J., Barlow, J., Baik, J. J., Belcher, S. E., Bohnenstengel, S. I., Calmet, I., Chen, F., Dandou, A., Fortuniak, K., Gouvea, M. L., Hamdi, R., Hendry, M., Kawai, T., Kawamoto, Y., Kondo, H., Krayenhoff, E. S., Lee, S. H., Loridan, T., Martilli, A., Masson, V., Miao, S., Oleson, K., Pigeon, G., Porson, A., Ryu, Y. H., Salamanca, F., Shashua-Bar, L., Steeneveld, G. J., Tombrou, M., Voogt, J., Young, D. and Zhang, N.: The international urban energy balance models comparison project: First results from phase 1, J.

https://doi.org/10.5194/gmd-2020-148
Preprint. Discussion started: 17 July 2020

Appl. Meteorol. Climatol., 49(6), 1268–1292, doi:10.1175/2010JAMC2354.1, 2010.

Hadka, D.: Platypus, [online] Available from: platypus.readthedocs.io (Accessed 13 February 2020), 2015.

Harshan, S., Roth, M., Velasco, E. and Demuzere, M.: Evaluation of an urban land surface scheme over a tropical suburban neighborhood, Theor. Appl. Climatol., 133(3–4), 867–886, doi:10.1007/s00704-017-2221-7, 2018.

Högström, U.: Non-dimensional wind and temperature profiles in the atmospheric surface layer: A re-evaluation, Boundary-Layer Meteorol., 42(1–2), 55–78, doi:10.1007/BF00119875, 1988.

Iwata, H., Hirata, R., Takahashi, Y., Miyabara, Y., Itoh, M. and Iizuka, K.: Partitioning Eddy-Covariance Methane Fluxes from a Shallow Lake into Diffusive and Ebullitive Fluxes, Boundary-Layer Meteorol., 169(3), 413–428, doi:10.1007/s10546-018-0383-1, 2018.

Järvi, L., Grimmond, C. S. B. and Christen, A.: The Surface Urban Energy and Water Balance Scheme (SUEWS): Evaluation in Los Angeles and Vancouver, J. Hydrol., 411(3–4), 219–237, doi:10.1016/j.jhydrol.2011.10.001, 2011.

Järvi, L., Grimmond, C. S. B., Taka, M., Nordbo, A., Setälä, H. and Strachan, I. B.: Development of the Surface Urban Energy and Water Balance Scheme (SUEWS) for cold climate cities, Geosci. Model Dev., 7(4), 1691–1711, doi:10.5194/gmd-7-1691-2014, 2014.

Järvi, L., Havu, M., Ward, H. C., Bellucco, V., McFadden, J. P., Toivonen, T., Heikinheimo, V., Kolari, P., Riikonen, A. and Grimmond, C. S. B.: Spatial Modeling of Local-Scale Biogenic and Anthropogenic Carbon Dioxide Emissions in Helsinki, J. Geophys. Res. Atmos., 2018JD029576, doi:10.1029/2018JD029576, 2019.

Karsisto, P., Fortelius, C., Demuzere, M., Grimmond, C. S. B., Oleson, K. W., Kouznetsov, R., Masson, V. and Järvi, L.: Seasonal surface urban energy balance and wintertime stability simulated using three land-surface models in the high-latitude city Helsinki, Q. J. R. Meteorol. Soc., 142(694), 401–417, doi:10.1002/qj.2659, 2016.

Kawai, T., Ridwan, M. K. and Kanda, M.: Evaluation of the simple urban energy balance model using selected data from 1-yr flux observations at two cities, J. Appl. Meteorol. Climatol., 48(4), 693–715, doi:10.1175/2008JAMC1891.1, 2009.

Kent, C. W., Grimmond, S. and Gatey, D.: Aerodynamic roughness parameters in cities:

https://doi.org/10.5194/gmd-2020-148
Preprint. Discussion started: 17 July 2020

Inclusion of vegetation, J. Wind Eng. Ind. Aerodyn., 169, 168–176, doi:10.1016/j.jweia.2017.07.016, 2017a.

Kent, C. W., Lee, K., Ward, H. C., Hong, J.-W., Hong, J., Gatey, D. and Grimmond, S.: Aerodynamic roughness variation with vegetation: analysis in a suburban neighbourhood and a city park, Urban Ecosyst., doi:10.1007/s11252-017-0710-1, 2017b.

Keyser, T. L., Lentile, L. B., Smith, F. W. and Shepperd, W. D.: Changes in Forest Structure After a Large, Mixed-Severity Wildfire in Ponderosa Pine Forests of the Black Hills, South Dakota, USA., 2008.

Kokkonen, T. V., Grimmond, C. S. B., Räty, O., Ward, H. C., Christen, A., Oke, T. R., Kotthaus, S. and Järvi, L.: Sensitivity of Surface Urban Energy and Water Balance Scheme (SUEWS) to downscaling of reanalysis forcing data, Urban Clim., 23, 36–52, doi:10.1016/j.uclim.2017.05.001, 2018.

Kowalczyk, E. A., Wang, Y. P. and Law, R. M.: The CSIRO Atmosphere Biosphere Land Exchange (CABLE) model for use in climate models and as an offline model, CSIRO Mar. Atmos. Res. Pap., 13(November 2015), 1–42, doi:https://doi.org/10.4225/08/58615c6a9a51d, 2006.

Krinner, G., Viovy, N., de Noblet-Ducoudré, N., Ogée, J., Polcher, J., Friedlingstein, P., Ciais, P., Sitch, S. and Prentice, I. C.: A dynamic global vegetation model for studies of the coupled atmosphere-biosphere system, Global Biogeochem. Cycles, 19(1), doi:10.1029/2003GB002199, 2005.

Kusaka, H., Kondo, H., Kikegawa, Y. and Kimura, F.: A Simple Single-Layer Urban Canopy Model For Atmospheric Models: Comparison With Multi-Layer And Slab Models, Boundary-Layer Meteorol., 101(3), 329–358, doi:10.1023/A:1019207923078, 2001.

Levis, S., Bonan, G. B., Vertenstein, M. and Oleson, K. W.: Technical Documentation and User's Guide to the Community Land Model's Dynamic Global Vegetation Model, , doi:10.5065/D6P26W36, 2004.

Liu, Y., Xie, R., Hou, P., Li, S., Zhang, H., Ming, B., Long, H. and Liang, S.: Phenological responses of maize to changes in environment when grown at different latitudes in China, F. Crop. Res., 144, 192–199, doi:10.1016/j.fcr.2013.01.003, 2013.

Loridan, T., Grimmond, C. S. B., Offerle, B. D., Young, D. T., Smith, T. E. L., Järvi, L. and

Lindberg, F.: Local-Scale Urban Meteorological Parameterization Scheme (LUMPS): Longwave Radiation Parameterization and Seasonality-Related Developments, J. Appl. Meteorol. Climatol., 50(1), 185–202, doi:10.1175/2010JAMC2474.1, 2011.

Margolis, H. A.: AmeriFlux CA-Qcu Quebec - Eastern Boreal, Black Spruce/Jack Pine Cutover, , doi:10.17190/AMF/1246828, 2001.

Martilli, A., Clappier, A. and Rotach, M. W.: An Urban Surface Exchange Parameterisation for Mesoscale Models, Boundary-Layer Meteorol., 104(2), 261–304, doi:10.1023/A:1016099921195, 2002.

Masson, V.: A physically-based scheme for the urban energy budget in atmospheric models, Boundary-Layer Meteorol., 94(3), 357–397, doi:10.1023/A:1002463829265, 2000.

McCaughey, J. H.: Energy balance storage terms in a mature mixed forest at Petawawa, Ontario - A case study, Boundary-Layer Meteorol., 31(1), 89–101, doi:10.1007/BF00120036, 1985.

McFadden J. P.: AmeriFlux US-KUT KUOM Turfgrass Field, , doi:10.17190/AMF/1246145, 2009.

Meyers and Tilden: AmeriFlux US-Blk Black Hills, , doi:10.17190/AMF/1246031, 2016.

Moene, A. F. and van Dam, J. C.: Transport in the Atmosphere-Vegetation-Soil Continuum, Cambridge University Press., 2013.

Monin, A. S. and Obukhov, A. M.: Basic laws of turbulent mixing in the surface layer of the atmosphere, Contrib. Geophys. Inst. Acad. Sci. USSR, 24(151), 163–187, 1954.

Monteith, J. L.: Evaporation and environment., Symp. Soc. Exp. Biol., 19(19), 205–34 [online] Available from: http://www.ncbi.nlm.nih.gov/pubmed/5321565 (Accessed 21 October 2019), 1965.

Myneni, R., Knyazikhin, Y. and Park, T.: MCD15A3H MODIS/Terra+Aqua Leaf Area Index/FPAR 4-day L4 Global 500m SIN Grid V006. NASA EOSDIS Land Processes DAAC, 2015.

Nations, U.: 2018 revision of world urbanization prospects, 2018.

Nishihama, M., Wolfe, R., Solomon, D., Patt, F., Blanchette, J., Fleig, A. and Masuoka, E.:

https://doi.org/10.5194/gmd-2020-148
Preprint. Discussion started: 17 July 2020

MODIS Level 1A Earth Location: Algorithm Theoretical Basis Document By the MODIS Science Data Support Team, Greenbelt, Md., 1997.

Noormets, A., McNulty, S. G., DeForest, J. L., Sun, G., Li, Q. and Chen, J.: Drought during canopy development has lasting effect on annual carbon balance in a deciduous temperate forest, New Phytol., 179(3), 818–828, doi:10.1111/j.1469-8137.2008.02501.x, 2008.

Nunez, M., Davies, J. A. and Robinson, P. J.: Surface albedo at a tower site in Lake Ontario, Boundary-Layer Meteorol., 3(1), 77–86, doi:10.1007/BF00769108, 1972.

Offerle, B., Grimmond, C. S. B. and Oke, T. R.: Parameterization of Net All-Wave Radiation for Urban Areas, J. Appl. Meteorol., 42(8), 1157–1173, doi:10.1175/1520-0450(2003)042<1157:PONARF>2.0.CO;2, 2003.

Omidvar, H., Sun, T. and Grimmond, C. S. B.: Assets for SUEWS Parameters calculation, , doi:10.5281/zenodo.3831233, 2020.

Penman, H. L.: Natural evaporation from open water, hare soil and grass, Proc. R. Soc. Lond. A. Math. Phys. Sci., 193(1032), 120–145, doi:10.1098/rspa.1948.0037, 1948.

Peters, E. B., Hiller, R. V. and McFadden, J. P.: Seasonal contributions of vegetation types to suburban evapotranspiration, J. Geophys. Res. Biogeosciences, 116(1), G01003, doi:10.1029/2010JG001463, 2011.

Philip Bloomington, R. and Novick Bloomington, K.: AmeriFlux US-MMS Morgan Monroe State Forest, , doi:10.17190/AMF/1246080, 2016.

Porter, C. L.: An Analysis of Variation Between Upland and Lowland Switchgrass, Panicum Virgatum L., in Central Oklahoma, Ecology, 47(6), 980–992, doi:10.2307/1935646, 1966.

Schmid, H. P., Grimmond, C. S. B., Cropley, F., Offerle, B. and Su, H. B.: Measurements of CO2 and energy fluxes over a mixed hardwood forest in the mid-western United States, Agric. For. Meteorol., 103(4), 357–374, doi:10.1016/S0168-1923(00)00140-4, 2000.

Shuttleworth, W. J.: A simplified one-dimensional theoretical description of the vegetation-atmosphere interaction, Boundary-Layer Meteorol., 14(1), 3–27, doi:10.1007/BF00123986, 1978.

Shuttleworth, W. J.: Evaporation models in the global water budget., Var. Glob. water Budg., 147–171, doi:10.1007/978-94-009-6954-4_11, 1983.

https://doi.org/10.5194/gmd-2020-148
Preprint. Discussion started: 17 July 2020

Spronken-Smith, R. A., Oke, T. R. and Lowry, W. P.: Advection and the surface energy balance across an irrigated urban park, Int. J. Climatol., 20(9), 1033–1047, doi:10.1002/1097-0088(200007)20:9<1033::AID-JOC508>3.0.CO;2-U, 2000.

Sun, T. and Grimmond, S.: A Python-enhanced urban land surface model SuPy (SUEWS in Python, v2019.2): development, deployment and demonstration, Geosci. Model Dev, 12, 2781–2795, doi:10.5194/gmd-12-2781-2019, 2019.

Sun, T., Järvi, L., Omidvar, H., Theeuwes, N., Lindberg, F., Li, Z. and Grimmond, S.: Urban-Meteorology-Reading/SUEWS: 2020a Release, , doi:10.5281/zenodo.3828525, 2020.

Van Ulden, A. P. and Holtslag, A. A. M.: Estimation of atmospheric boundary layer parameters for diffusion applications., J. Clim. Appl. Meteorol., 24(11), 1196–1207, doi:10.1175/1520-0450(1985)024<1196:EOABLP>2.0.CO;2, 1985.

Ward, H. C., Kotthaus, S., Järvi, L. and Grimmond, C. S. B.: Surface Urban Energy and Water Balance Scheme (SUEWS): Development and evaluation at two UK sites, Urban Clim., 18, 1–32, doi:10.1016/j.uclim.2016.05.001, 2016.

Zhou, A., Qu, B.-Y., Li, H., Zhao, S.-Z., Suganthan, P. N. and Zhang, Q.: Multiobjective evolutionary algorithms: A survey of the state of the art, Swarm Evol. Comput., 1(1), 32–49, doi:10.1016/j.swevo.2011.03.001, 2011.